Article:
Zhang, B., Ma, X., Liu, L. et al. (4 more authors) (2024) Reciprocating sliding friction behavior and wear state transition mechanism of cylinder liner and piston ring. Wear, 546-547. 205293. ISSN 0043-1648

https://doi.org/10.1016/j.wear.2024.205293

Reciprocating sliding friction behavior and wear state transition mechanism of cylinder liner and piston ring

Baofeng Zhang[1], Xuan Ma[1*], Lining Liu[2], Yongqiang Wang[1], Hanzhengnan Yu[3], Ardian Morina[4], Xiqun Lu[1*]

1. College of Power and Energy Engineering, Harbin Engineering University, Harbin, China;
2. College of Mechanical and Electrical Engineering, Harbin Engineering University, Harbin, China;
3. China Automotive Technology and Research Center Co., Ltd., Tianjin, China;
4. School of Mechanical Engineering, University of Leeds, Leeds, UK;

Corresponding authors: Xuan Ma, Associate professor;

E-mail: maxuan@hrbeu.edu.cn

Xiqun Lu, Professor;

E-mail: luxiqun@hrbeu.edu.cn

Highlights:

- The friction and wear characteristics of cylinder liner piston rings under harsh conditions were studied by dry friction experiment.
- The mechanism of wear state transition is analyzed from the perspective of microstructure.
- The time-varying characteristics of the cylinder liner cast iron material wear process are analyzed.
- The wear and degradation process of cylinder liner cast iron is revealed from the microstructure perspective.

Abstract:

To investigate the wear time-varying characteristics of cylinder liner cast iron, dry sliding wear experiments were conducted on the cylinder liner and piston ring at room temperature. The surface and interface morphologies of the cylinder liner wear scar were analyzed using a white light interferometer, scanning electron microscope (SEM), and transmission electron microscope (TEM) at different wear times. The results indicate that the wear state of cylinder liner cast iron changes over time. Based on the change in friction coefficient, the wear process can be divided into three stages: low wear stage, stable wear stage, and severe wear stage. The shedding of graphite and its self-lubricating effect contributes to the low friction coefficient and wear rate observed in the low wear stage. The formation of a friction layer leads to the wear entering a stable stage, where adhesive wear of pearlite occurs. As the friction layer and the phosphorus eutectic wear and fall off, the wear process of the cylinder liner intensifies, with delamination wear becoming the primary wear mechanism. This study reveals the wear degradation mechanism of cylinder liner cast iron from the perspective of microstructures, offering valuable information for predicting wear and optimizing the microstructure of cylinder liners and piston rings.

Keywords: Cylinder liner cast iron, Sliding wear, Microstructure, Wear stage

1. Introduction

The cylinder liner and piston ring are crucial friction pairs within the internal combustion engine, together with the piston, cylinder block, and cylinder head, forming a closed combustion space and playing a sliding sealing role. Research findings show that the frictional interaction between the cylinder liner and piston ring contributes to more than 20% of the overall mechanical loss experienced by internal combustion engines [1, 2]. When the internal combustion engine operates, the piston ring and cylinder liner experience wear, which frequently causes a reduction in cylinder air tightness and combustion efficiency. As a result, friction power consumption significantly increases while the engine's lifespan decreases. Particularly in the vicinity of the compression and power stroke's top dead center (TDC), forming a

comprehensive lubricating oil film becomes difficult due to the substantial combustion pressure and reduced sliding speed, the area with the highest friction and most severe wear. The cylinder liner scuffing generally occurs in this area [3, 4]. Hence, investigating the frictional characteristics and wear mechanisms of cylinder liners and piston rings in extreme operational environments is crucial for augmenting the dependability and longevity of internal combustion engines.

The wear process of the cylinder liner and piston ring is intricate due to the severe conditions they encounter, including elevated temperatures, pressures, and repetitive impacts. There are many reports on cylinder liner and piston ring wear processes. The prevailing belief suggests that the primary mechanisms responsible for cylinder liner wear include abrasive wear, adhesive wear, and corrosive wear, all of which manifest concurrently during operation. [5, 6]. Abrasive wear mainly refers to the wear caused by scratching hard particles between the friction pairs on the contact surface. The sources of hard particles mainly include dust drawn into the cylinder with air [7], carbon smoke generated by incomplete combustion [8, 9], and wear debris [10]. Generally, the wear rate caused by abrasive wear is low in the cylinder liner and piston ring, which belongs to mild wear. The corrosion wear behavior of the cylinder liner is related to factors such as fuel, sulfur content, lubricating medium, and environment [11, 12]. Especially the presence of sulfur will form sulfuric acid on the cylinder wall, leading to a corrosive environment and accelerating the wear process. Due to the high sulfur content in diesel, corrosion wear is one of the primary wear forms of marine engine cylinder liners and piston rings. In addition, the oxygen and water in the cylinder will react with the wear debris and form a dense oxide layer or glazed layer on the surface under the rolling action of the friction pair. The general consensus is that the formation of the glazed layer can prevent adhesive wear and improve wear resistance. At the same time, it can also cover the original irregular surface, making the mating surface smoother [13, 14]. However, some studies also have shown that when the thickness of the protective oxide film reaches the critical size, it will be removed, resulting in severe wear [15]. For many years, it has been believed that the high wear rate of cylinder liners and piston rings is related to corrosion wear, but most of the research results indicate

that corrosion wear is not the main cause of severe wear. However, adhesive wear is often one of the causes of severe wear. Although the cylinder liner and piston ring operate in a lubricated environment and the lubricating oil film can effectively isolate direct contact between the friction pair, the adhesion still exists. One of the main characteristics of the adhesion phenomenon is the high wear rate and unstable friction coefficient, and it even directly prevents the sliding process of the friction pair in severe cases [16]. Although adhesive wear is generally considered the main cause of the high wear rate of cylinder liners, this wear form mainly depends on the operating conditions rather than the cylinder liner material itself [5, 6, 17, 18]. Especially when the cylinder liner and piston ring are experiencing lubrication deficiency, as the wear process continues, the transformation of the wear mechanism can cause an alteration in the wear state. However, a consensus regarding this transition mechanism in the cylinder liner remains elusive.

Cast iron has high strength, thermal conductivity, and outstanding ability to withstand wear, extensively used in cylinder liner materials [19]. The type, morphology, and quantity of cast iron material's microstructure significantly impact its wear resistance [20-23]. Generally speaking, the matrix microstructure of cylinder liner cast iron is mainly pearlite. The lamellar dual-phase structure composed of brittle phase cementite and ductile phase ferrite gives the pearlite excellent wear resistance. It mainly manifests in two aspects: First, as a ductile phase in pearlite, ferrite can absorb friction energy and reduce cracking tendency. The brittle cementite can resist asperity penetration, so the pearlite has a lower wear rate [24]. On the other hand, the pearlite will undergo plastic deformation during friction, decreasing lamellar spacing or grain refinement, which improves the mechanical properties while also causing changes in wear mechanism and wear rate [25-27]. Some research has shown that for the layered pearlite, a glaze protective layer with self-lubricating properties is formed during the wear process due to the attachment of compacted oxides on the surface, resulting in a decrease in the friction coefficient and an enhancement in wear resistance [28].

Graphite is another significant microstructure in cylinder liner cast iron, with the capability to effectively enhance the properties of friction and wear. It is mainly

manifested in three aspects: Firstly, during the friction process, graphite will be squeezed out to the sliding surface due to the friction. The formed graphite film can effectively isolate the contact between the friction pairs, thereby decreasing both the friction coefficient and the wear loss [29, 30]. The above research mainly describes the self-lubricating effect of graphite in a dry friction state. In the lubrication state, graphite can also improve the friction performance. Graphite is prone to fall off during friction, resulting in the formation of pits on the wear scar surface. These pits can store more lubricating oil and improve friction performance under starved lubrication conditions [31]. Another important role of graphite is to improve the thermal conductivity of cast iron. Usually, friction heat can reduce the material's hardness and thermal fatigue properties, thus affecting the transition of the wear state [32]. Moreover, graphite can improve the heat conduction efficiency of cast iron, thereby improving wear resistance. Especially the morphology of graphite seriously affects the thermal conductivity of cast iron. Some researchers have shown that the thermal conductivity decreases significantly when the graphite morphology changes from layered to spherical [33, 34]. While the aspects above showcase the enhancement of wear resistance in cast iron due to graphite, some studies have also shown that graphite is often one of the causes of cast iron wear. Due to the poor adhesion between graphite and matrix structure, it becomes susceptible to erosion, resulting in pits on the wear scars. These pits provide the optimal location for the generation of cracks, which leads to the wear of the matrix structure [23, 35, 36]. In addition, graphite does not always play a self-lubricating role during the wear process. Some studies have shown that the lamellar graphite will close due to the deformation of the matrix structure during the wear process [23, 37]. And then lose the self-lubricating effect.

For cylinder liner cast iron, in order to improve its hardness and wear resistance, alloying elements are usually added to the cast iron to form a hard phase with high hardness [38, 39]. The matrix structure experiences decreased wear due to the supportive function of these hard phases in the wear process. On the other hand, abrasive wear is enhanced as the hard phase separates and generates abrasive particles that infiltrate the wear scar site [40]. From a microscopic point of view, the process of

cylinder liners experiencing wear is essentially the shedding process of their microstructures. Hence, the wear mechanism and the transformation of the wear state are significantly influenced by the microstructure of cast iron. However, most studies mainly focus on the role of a single microstructure in the wear process, making it difficult to explain the time-varying characteristics of cylinder liners during the wear process. Therefore, analyzing the synergistic effect of microstructures at different wear stages can more intuitively reveal the cylinder liner cast iron's wear mechanism.

This study focuses on the cylinder liner and piston ring as the research object and conducts an enhanced wear experiment using a multifunction tribology testing machine. The wear process of the cylinder liners is divided into different stages by observing the variation characteristics of friction coefficient and wear rate over time. Then, the surface and interface morphology of cylinder liners at different wear stages were analyzed, and the wear mechanism and microstructure wear characteristics of cylinder liners were discussed to clarify the synergistic effect of different microstructures in the wear process. At the same time, it also reveals the cylinder liner cast iron's wear degradation mechanism. This study investigates the transition of wear states of cylinder liners under harsh working conditions from a microstructural perspective. It examines the time-varying wear characteristics of the microstructure during the wear process of cylinder liners. It can contribute to the theoretical basis for the wear prediction of cylinder liners and the microstructure optimization of wear-resistant cast iron.

2. Experimental procedure

2.1. Materials and sample preparation

The samples in this study were taken from a new cylinder liner and piston rings with a cylinder diameter of 170 mm, and their chemical composition measured by a photoelectric direct reading spectrometer is shown in Table 1. The microstructure of the cylinder liner and piston ring is shown in Fig. 1. The cylinder liner material is gray cast iron with flake graphite, specifically type A. The matrix structure consists of pearlite, with a small amount of binary phosphorus eutectic distributed on the surface [41]. The piston ring is made of ductile cast iron and has a microstructure of tempered sorbite.

Additionally, the surface is coated with an amorphous Cr-C-Al alloy, and the chemical composition is shown in Table 1, which has a thickness of approximately 150 μm.

Wire electrical discharge machining (WEDM) was used to cut the cylinder liner into a cuboid of 30*15*6 mm. It can obtain a flat friction surface and avoid edge running since the diameter of the rings is usually larger than the corresponding cylinders. At the same time, it also avoids the influence and observation of the surface texture of the cylinder liner on the microstructure wear process. The piston ring was cut into a ring section with a length of 15 mm (Fig. 2). In order to observe the shedding of microstructures during the wear process and avoid the influence of surface roughness, 400#, 1000#, 2000#, and 3000# diamond sandpaper were used to grind the cylinder liner samples and then polished to obtain a smooth surface with roughness Ra ≤ 0.2. It can eliminate the interference of surface morphology in the experimental process.

Table1 Chemical composition of the cylinder liner and piston ring (wt%)

Elements	C	Si	Mn	P	Cr	Al	Cu
Cylinder liner	3.07	1.85	0.78	0.501	0.3	<0.01	0.407
Piston ring	3.52	2.77	0.247	0.04	<0.01	<0.01	0.51
Coating	7.45	0.18	<0.01	<0.01	88.95	0.64	<0.01

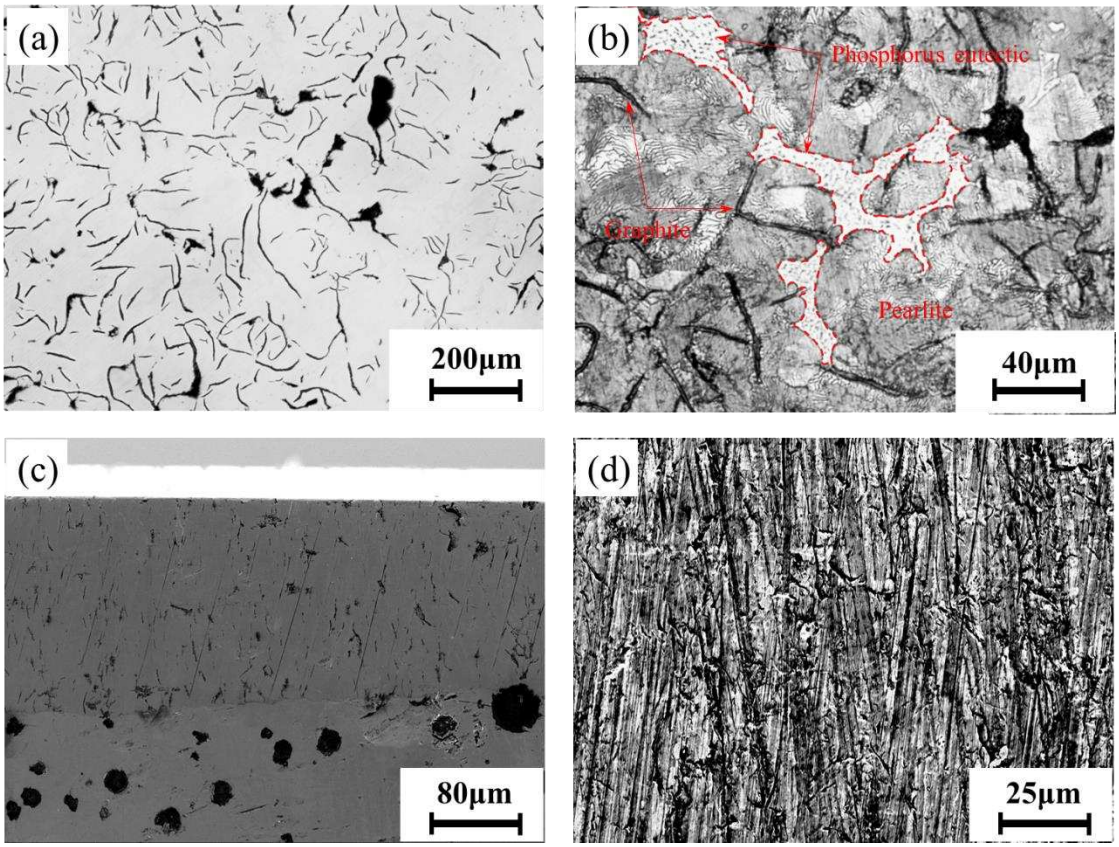

Fig. 1. Microstructure and morphology characteristics of the cylinder liner and piston ring: (a) cylinder liner graphite morphology, (b) cylinder liner microstructure, (c) piston ring cross-section morphology, (d) piston ring surface morphology.

2.2. Wear experiments

The reciprocating sliding wear experiment was conducted on a multifunction tribology testing machine (MFT5000, Rtec Instruments, USA). The experimental setup and sample dimensions are illustrated in Fig. 2. During the experiment, the piston ring sample was fixed in the upper fixture and remained stationary, and the vertical downward load was applied to the piston ring through the upper fixture. One end of the horizontal connecting rod was fixed on the fixture, and the other was connected to the friction sensor to record the friction in real time during the experiment. The cylinder liner sample was fixed on the lower test bench and performed periodic reciprocating motion with the test bench during the experiment. The principles of experimental equipment and fixtures have been explained in detail in previous studies [42].

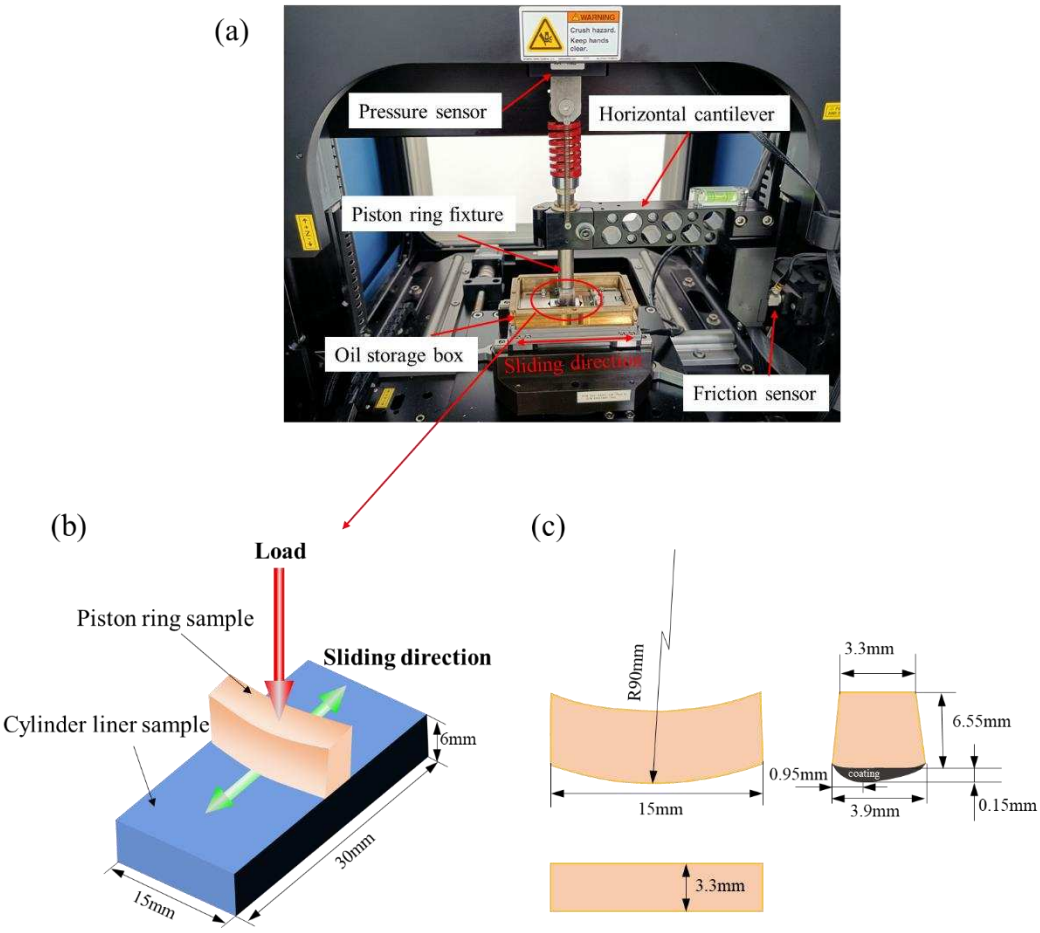

Fig. 2. Experimental principle and sample size: (a) testing machine, (b) experimental principle and cylinder liner sample size, (c) piston ring sample size and three views.

This study is particularly interested in the time-varying wear characteristics of the cylinder liner and piston ring under starved lubrication or more harsh working conditions. To simulate these conditions and accurately measure wear changes at different stages of the experiment, a dry friction experiment was conducted. This experiment accelerated and intensified the wear process, thereby shortening the experimental cycle. Due to cooling reasons, the actual engine cylinder wall temperature is generally about 100-200 °C [43]. Usually, we believe that the temperature mainly affects the wear process by affecting the viscosity of the lubricating oil. As this study adopts the dry friction experiment and ignores the influence of temperature, the test temperature is set at room temperature. The experimental load is 50 N, and based on the piston ring size, it can be determined that the load is approximately 1 MPa cylinder

pressure in the actual engine. In accordance with the Hertz contact theory [44], the average contact pressure of the cylinder liner and piston ring is about 132 MPa, which aligns with the findings documented in the literature [45]. The experiment reciprocating sliding frequency is 2 Hz, consistent with the piston's speed range at the top dead center position in our previous research [42]. The stroke is 20 mm, and the experimental time is 3 h. To investigate the wear mechanism at various stages, the wear loss of different periods was obtained at an interval of 30 min. Due to the friction coefficient changes significantly in the first 60 min, the experimental interval within the first 60 min is 15 min. The wear experimental time is 15 min, 30 min, 45 min, 60 min, 90 min, 120 min, 150 min, and 180 min respectively. The wear debris on the sample was collected before measurement, and the sample was ultrasonically cleaned with anhydrous ethanol for 10 min. Then, the wear loss and wear scar morphology were characterized. To ensure the accuracy of the test results, each wear test was repeated three times.

2.3. Calculation of wear volume

It is crucial to determine the wear amount at different time intervals to analyze the variation in wear rate. However, accurately measuring the wear mass through weighing methods is challenging due to the small amount of wear occurring during the experiment. Therefore, this study calculates the wear volume to determine the wear amount at different time intervals. The calculation method of cylinder liner and piston ring wear volume refers to the calculation model reported in relevant literature [46]. Fig. 3 shows the shape and three views of the piston ring wear scar. The diameter of the piston ring in a free state is 180 mm, and the external profile is a trapezoidal barrel. The fitting equation of the external profile is shown in equation 1. The piston ring surface has a compound curvature, the initial circumferential curvature is R_o, and the circumferential curvature after wear is R_w. The initial axial curvature boundary is the curve $f_o(y)$, and the curvature boundary after wear is $f_w(y)$ (equation 2). W is the width of the wear scar, which is the same as the width of the wear scar on the surface of the cylinder liner sample. The above parameters can be obtained through data fitting after measurement with a white light interferometer.

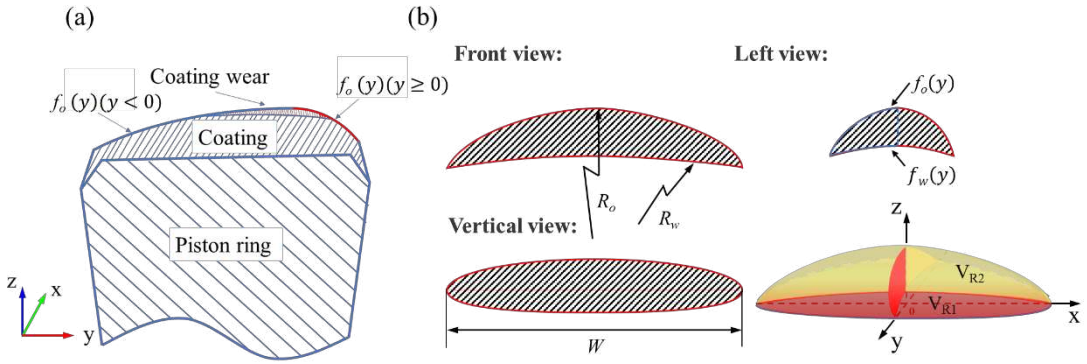

Fig. 3. Wear shape and three views of piston ring coating: (a) wear cross-section morphology of piston ring coating, (b) wear shape and three views of piston ring.

$$f_o(y)=\begin{cases}-0.1y^2+R_o-\sqrt{{R_o}^2-\dfrac{W^2}{4}} & (y\geq 0)\\ -0.013y^2+R_o-\sqrt{{R_o}^2-\dfrac{W^2}{4}} & (y<0)\end{cases} \tag{1}$$

$$f_w(y)=\begin{cases}ay^2+R_w-\sqrt{{R_w}^2-\dfrac{W^2}{4}} & (y\geq 0)\\ by^2+R_w-\sqrt{{R_w}^2-\dfrac{W^2}{4}} & (y<0)\end{cases} \tag{2}$$

Where, a and b are both fitting coefficients. The profile of the piston ring is an asymmetric barrel surface shape, the wear volume on the left and right sides of the axial direction is not equal (Fig. 3 (b)), so, the wear volume is divided into two parts for calculation. According to the calculation method reported in the literature [46], the wear volume of the piston ring can be obtained by the equation 3 through numerical integration.

$$V_{Ring}=f\left(W,R_o,f_o(y)\right)-f\left(W,R_w,f_w(y)\right) \tag{3}$$

$$f\left(W,R,f(y)\right)=\int_0^c\left[\frac{\pi d^2 arc\cos\left(\frac{h}{d}\right)}{180}-h\sqrt{d^2-h^2}\right]dy \tag{4}$$

Where, c is the maximum wear scar width in the axial direction of the piston ring. Due to the asymmetry of the profile, the maximum wear scar width on the left and right sides of the maximum outer diameter of the piston ring is different, which can be

calculated according to equation 5. d_o and d_w are the radius of the piston ring at different axial positions before and after wear, which can be obtained by equation 6 and 7 respectively. h is the distance from the center point of the piston ring to the horizontal plane of the lowest point of the wear scar, which can be calculated by equation 8.

$$c = \begin{cases} \sqrt{10}\sqrt{R_o - \sqrt{{R_o}^2 - \frac{W^2}{4}}} & (y \geq 0) \\ -10\sqrt{\frac{10}{13}}\sqrt{R_o - \sqrt{{R_o}^2 - \frac{W^2}{4}}} & (y < 0) \end{cases} \tag{5}$$

$$d_o = \begin{cases} R_o - 0.1y^2 & (y \geq 0) \\ R_o - 0.013y^2 & (y < 0) \end{cases} \tag{6}$$

$$d_w = \begin{cases} R_w + ay^2 & (y \geq 0) \\ R_w + by^2 & (y < 0) \end{cases} \tag{7}$$

$$h = \sqrt{{R_o}^2 - \frac{W^2}{4}} \tag{8}$$

Fig. 4 shows the wear scar shape and three views of the cylinder liner sample. The wear volume of the cylinder liner is divided into three parts: one part is the wear caused by the sliding of the piston ring and the cylinder liner in the stroke. The other two parts are the wear caused by the axial thickness of the piston ring at both ends of the wear scar. This is, the wear volume of the cylinder liner is calculated by equation 9, and the wear scar volume on the stroke is calculated by equation 10. After the wear experiment, the cross-sectional morphology was measured at three different positions (the middle and both ends of the stroke) by the white light interferometer to obtain the cross-sectional area of the wear scars. The average cross-sectional area obtained from three measurements is used to calculate the wear volume on the stroke length. The morphology at both ends of the wear scar on the cylinder liner has the same composite curvature as the piston rings, according to the above measured morphological characteristics of the piston ring after wear, the wear volume caused by the axial curvature of the piston ring at both ends of the wear scar can be obtained by equation 11 and equation12.

$$V_c = V_l + V_{l1} + V_{l2} \tag{9}$$

$$V_l = \bar{S}l \tag{10}$$

$$V_{l1} = f\left(W, R_w, f_w(y)\right) \quad (y < 0) \tag{11}$$

$$V_{l2} = f\left(W, R_w, f_w(y)\right) \quad (y \geq 0) \tag{12}$$

Where V_c is the total wear volume of the cylinder liner, V_l is wear volume on stroke length, V_{l1}, V_{l2} is the wear volume caused by the axial curvature of the piston ring at the end of the stroke, $\bar{S}$ is the average cross-sectional area, l is the sliding stroke.

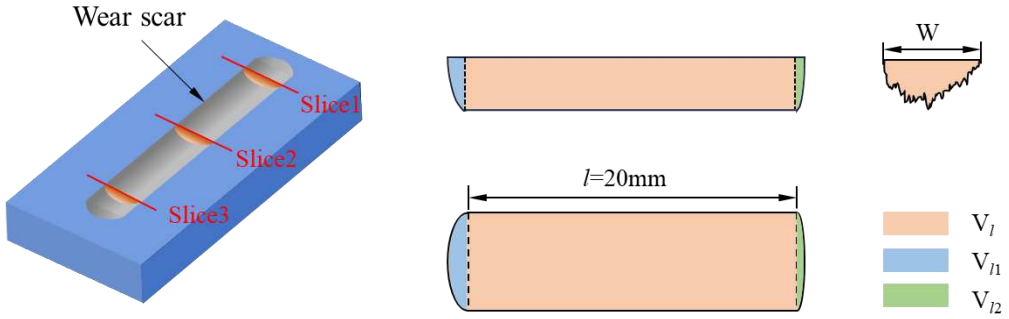

Fig. 4. Cylinder liner wear scar schematic diagram and its shape three views.

2.4. Analysis of wear scar morphology

The optical microscope (OM) was used to analyze the cylinder liner and piston ring microstructure composition. To examine the wear volume and roughness variations of these components, a white light interferometer (Zegage, Zygo) was employed to measure the surface morphology of the wear scar. Scanning electron microscopy (SEM) and X-ray energy dispersive spectroscopy (EDS) were used to characterize the morphology of wear debris, surface and cross-sectional morphology of wear scars, and element distribution to analyze the wear mechanisms at different wear stages. The focused ion beam technique (FIB) was used to cut thin slices at the wear scar position to prepare TEM samples. The microstructure of the wear scar cross-section was observed by transmission electron microscopy (TEM) and high-resolution transmission electron microscopy (HRTEM), and the morphology and characteristics of the layered structure of the wear scar cross-section were analyzed.

3. Results

3.1. Evolution of friction behavior

Fig. 5 depicts the alterations in the friction coefficient throughout various durations of experimentation. The large amplitude of the friction coefficient caused by reciprocating friction affects the analysis of the experimental results. Therefore, Fig. 5 (a) results from fourier low-pass filtering (cut-off frequency is 0.5). Fig. 5 (b) and Fig. 5 (c) are the local enlarged images of positions A and B in Fig. 5 (a), respectively. The observation reveals an upward trend in the friction coefficient as time progresses. Initially, the friction coefficient was minimal and experienced significant growth within a brief duration, subsequently maintaining stability between 0.2-0.3. Furthermore, the data indicates a steady decline in the friction coefficient during a relatively stable phase (Fig. 5 (b)). Subsequent to the initial 15 min, the friction coefficient exhibited progressive increments, plateauing at an elevated level. It is worth noting that the friction coefficient also shows a decreasing process before reaching stability (Fig. 5 (c)), which may be related to the self-lubricating properties of the material. The friction process in steel materials leads to the formation of a nanocrystalline layer comprised of Fe oxides on the wear scar surface due to the repetitive rolling of grinding debris. This layer effectively diminishes both the friction coefficient and wear rate [47, 48]. Furthermore, observable evidence indicates that the friction coefficient gradually increases and stabilizes after initially decreasing. The amplitude fluctuation also gradually increases, indicating that there may be severe wear on the contact surface at this time. Finally, after a period of stability, the friction coefficient increases again and remains stable when the value approaches 0.6. Fig. 5 (d) is the average variation of friction coefficient in different periods (with a time interval of 15 min) and the standard deviation of three repeated tests. It can be seen more clearly that the friction coefficient changes with the experiment time. The process is divided into five stages: stages 1, 3, and 5 are the stable stage of friction coefficient, and stages 2 and 4 are the rising stage (Fig. 5 (d)). In the first stage, the friction coefficient is relatively low (< 0.3), and the stability time is short (about 15 min), which is called the low wear stage. In the third stage, the friction coefficient is stable between 0.35 and 0.45, and the duration is about

45 min, which is called the stable wear stage. The friction coefficient of the fifth stage is stable between 0.5-0.6, which is called the severe wear stage. Furthermore, the decrease of friction coefficient in Fig. 5 (b) (c) occurs in the low and stable wear stages, and this phenomenon explains the lower average friction coefficient at the beginning of the stable wear stage (Fig. 5 (d)).

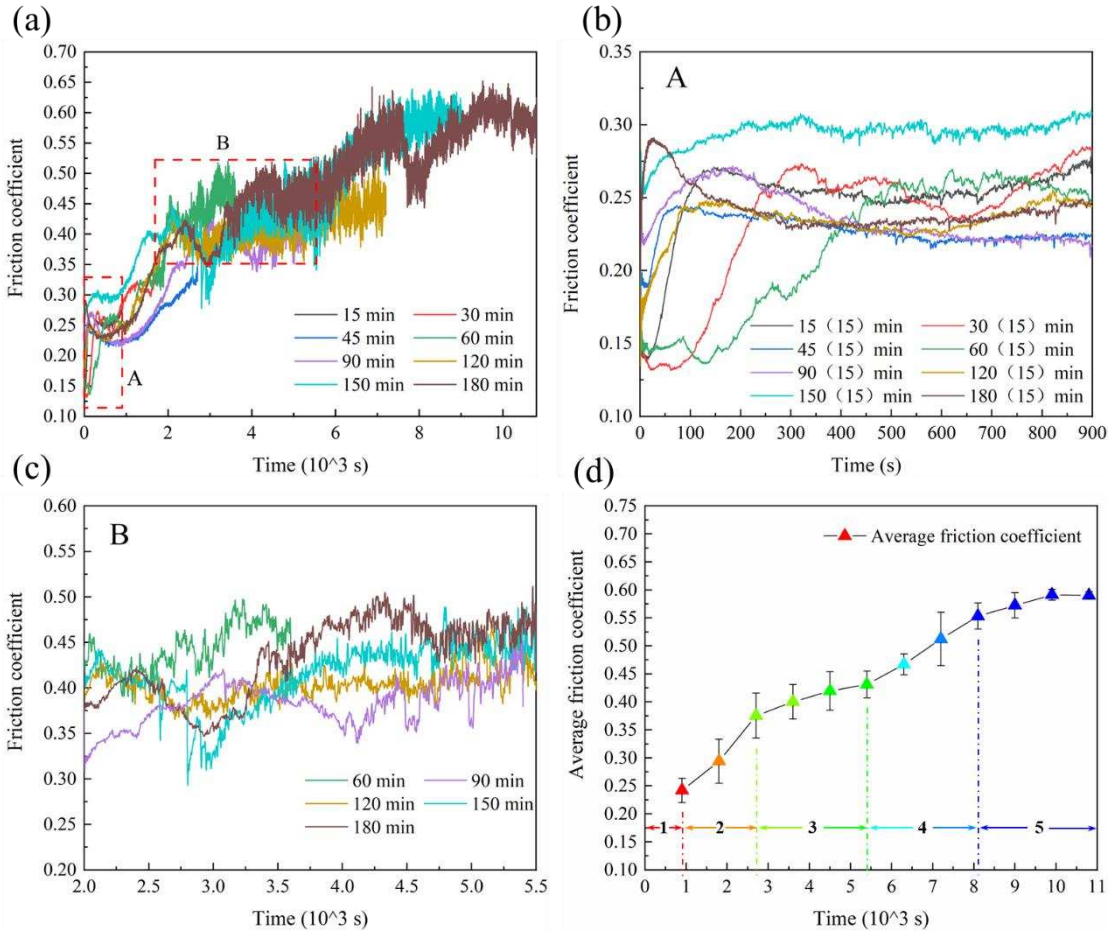

Fig. 5. The variation of friction coefficient: (a) the variation of friction coefficient at different wear times, (b) the local enlarged image of position A in Fig (a) (friction coefficient variation during different experiments in the first 15 min), (c) the local enlarged image of position B in Fig. (a) (after low-pass filtering processing, with a cutoff frequency of 0.1), (d) the variation of the average value of friction coefficient in different periods (taking the average value every 15 min).

3.2. Wear behaviour

In order to analyze the wear of the cylinder liner and piston ring at different periods, the wear scars of the cylinder liner were analyzed by white light interferometer. Fig. 6

displays the cross-section characteristics of wear scars of cylinder liner at different wear times. According to the variation of friction coefficient, it is low within the first 15 min and then gradually rises. It can also be seen from the cross-section morphology of the wear scar in the first 30 min that the depth is shallow, indicating that the surface wear is slight at this time. There are also apparent protrusions on the surface, mainly formed by the adhesion of the wear debris. As the wear process progresses, the depth of the wear scar gradually increases. When the wear time is 60 min, according to Fig. 5 (d), the friction coefficient reaches the second stable state. It can be seen from the cross-section of the wear scar that the surface protrusion is significantly reduced, indicating that the surface is deformed or worn, and the adhesion of the wear debris is not enough to produce protrusions. The cross-sectional morphology of the wear scar at a wear time of 90 min is similar to that at 60 min, and the morphology distribution at the bottom of the wear scar is not uniform. When the wear time is 150 min, according to the change of friction coefficient (Fig. 5 (c)), the friction coefficient reaches the maximum and remains stable. At this time, the depth of the wear scar changes little while the width changes significantly. When the wear time is 180 min, the cross-section of the wear scar is uniform and smooth.

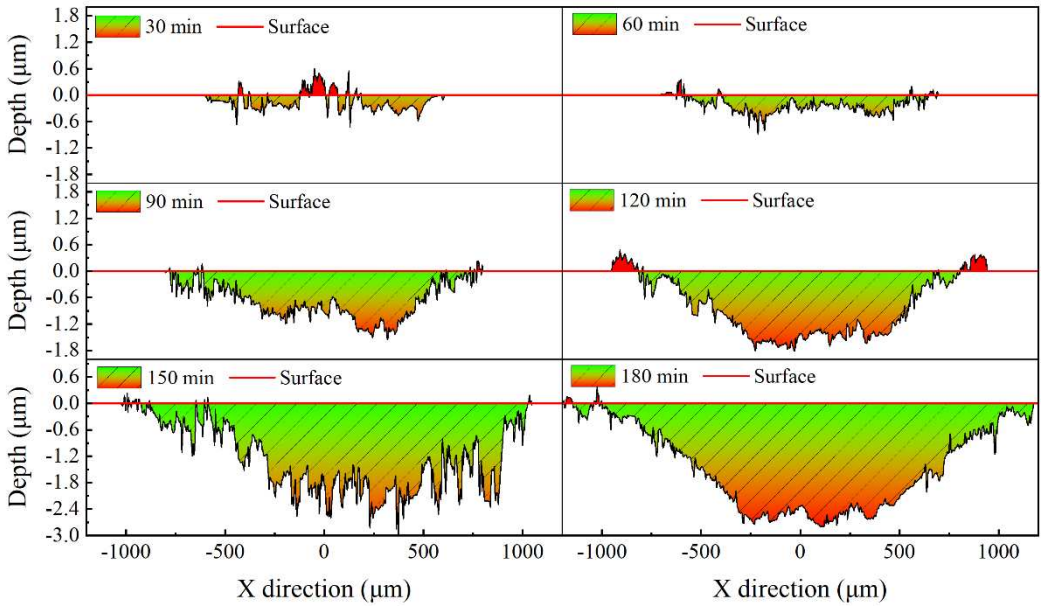

Fig. 6. Cylinder liner wear scar cross-section morphology.

Fig. 7 shows the average value and standard deviation of the three tests' calculation

results of the wear volume of the cylinder liner and piston ring at different periods. It can be seen that the wear volume of the cylinder liner and piston ring increases with time, and the wear volume of the cylinder liner is much greater than that of the piston ring, which is consistent with the results reported in the literature [49]. In the initial 60 min, the wear of both the cylinder liner and piston ring is minimal. However, after reaching 90 min of wear time, there is a noticeable increase in the wear of the piston ring and cylinder liner. This observation strongly suggests that the wear state of the cylinder liner undergoes a significant alteration after the initial 60 min period. According to the change of friction coefficient, the friction coefficient is in the second stable stage at 60 min, and the self-lubricating phenomenon has just been completed. That is, the friction coefficient will rise slightly after 60 min. With the increase of wear time, the wear volume of the piston ring also increased obviously.

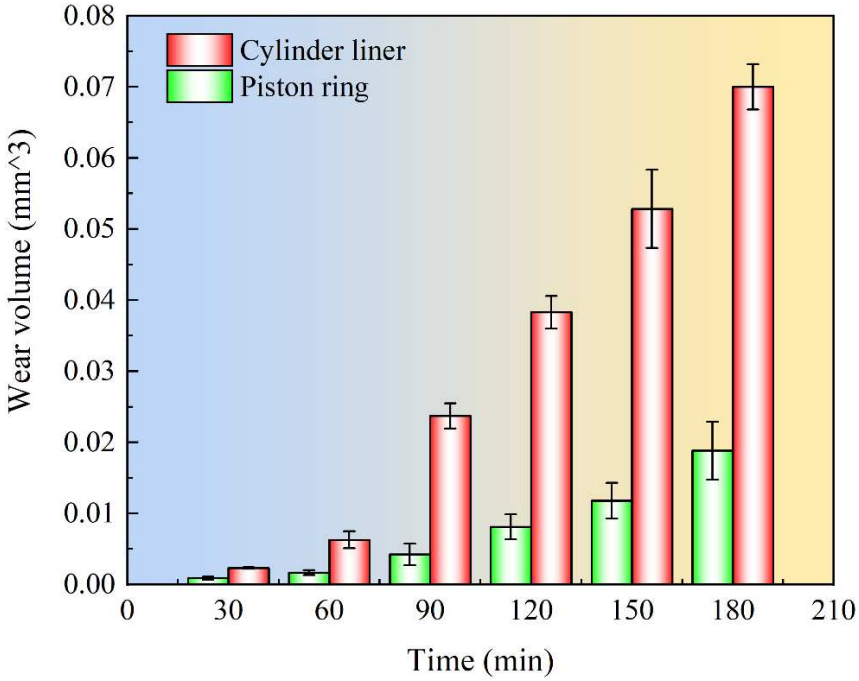

Fig. 7. Wear volume of cylinder liner and piston ring under different wear time

In order to clearly describe the changes in the wear rate of cylinder liners and piston rings at different periods, the wear rates were calculated by equation 13[50].

$$k = \frac{\Delta V}{A_n L} \tag{13}$$

Where k is the normalized wear rate, ΔV is the wear volume within 30 min at different times, A_n is the is the nominal contact area, and L is the sliding distance.

Fig. 8 illustrates the temporal evolution of the wear rate for both the cylinder liner and piston ring. It can be seen from the figure that the cylinder liner wear rate generally increases first and then tends to be stable. When the wear time is less than 90 min, the wear rate increases with time. When the wear time is greater than 90 min, the wear rate is higher and tends to be stable. In addition, it can be seen from the wear rate changes at 150 min and 180 min that there seems to be a periodic change process in the severe wear stage. That is, the wear rate is relatively high for a while (120-150 min), followed by a decrease in wear rate for another period (150-180 min). However, it remained relatively stable, with a stable value of about 6.5E-8. In comparison to the wear rate of the cylinder liner, the wear rate exhibited by the piston ring is lower. The wear rate of the piston ring is stable during the whole wear process. Despite observing variations in wear rates over different time intervals, these differences are relatively insignificant. This could be attributed to the remarkable hardness and homogeneous microstructure of the Cr-C-Al coating applied on the surface of the piston ring [51]. During the wear process, the mechanism remains unaltered, thereby resulting in a relatively minimal shift in the wear rate. In other words, the state of the piston ring's wear predominantly relies on the experimental parameters instead of the experimental duration [52].

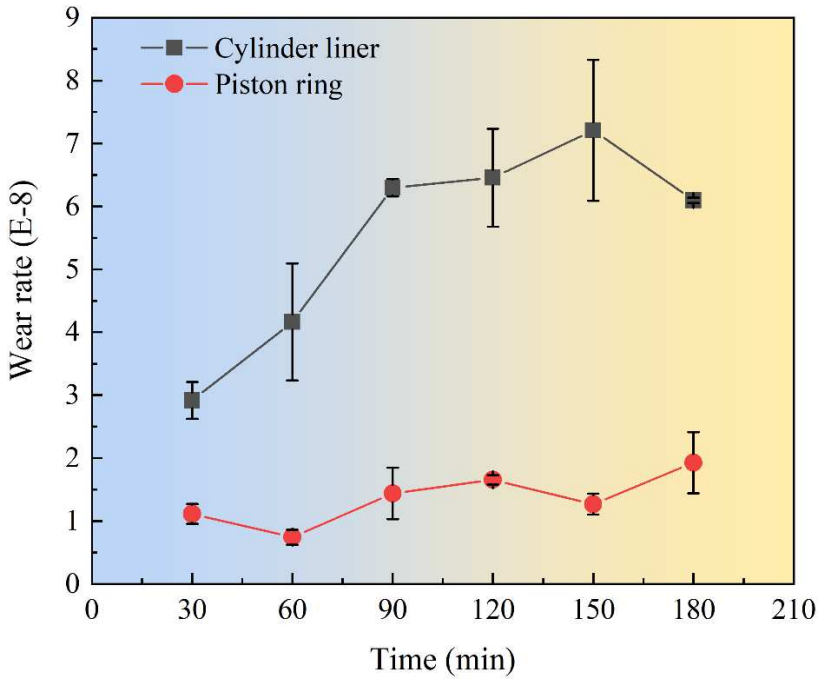

Fig. 8. Wear rate of cylinder liner and piston ring in different wear periods.

3.3. Evolution of surface roughness

The friction coefficient and wear rate between friction pairs are significantly influenced by the surface morphology. Considering the microscopic viewpoint, increasing surface roughness results in higher friction coefficient and more pronounced wear. Fig. 9 illustrates the changes in the two-dimensional and three-dimensional structure of the cylinder liner surface as wear progresses. In the two-dimensional analysis, there is a gradual darkening in the color of the wear scar region, possibly indicating oxidation or graphite overflow. Similarly, the three-dimensional analysis reveals that the wear scar surface is initially smooth after 30 min. However, a slight protrusion appears in the center due to the accumulation of wear debris, matching the findings presented in Fig. 6. As the duration of wear prolongs, an escalation in the manifestation of flaws on the eroded surface occurs (Fig. 9 (b2)). This phenomenon, in turn, accounts for the observed rise in the friction coefficient. However, it is worth noting that the wear scar exhibits a minimal depth, primarily resulting from the shedding of the superficial microstructure. When the wear time is 90 min, the surface roughness, wear depth and rate increase. When the wear time is 150 min, a significant occurrence of spalling is observed on the wear scar's surface, indicating that the wear mechanism changes at this time, which will also lead to a further increase in surface roughness. Based on the previous analysis of the friction coefficient and wear rate, it can be seen that the friction coefficient and wear rate values are both high at this time. Fig. 10 shows the variation of surface roughness Sa of cylinder liner and piston ring wear scars at different times. It can be seen from the figure that the surface roughness of the cylinder liner increases with time. The roughness of the piston ring surface shows periodic changes, and the change range is much smaller than that of the cylinder liner. It indicates that the wear state of the piston ring during the experiment is relatively stable, which is consistent with the variation in its wear rate (Fig. 8).

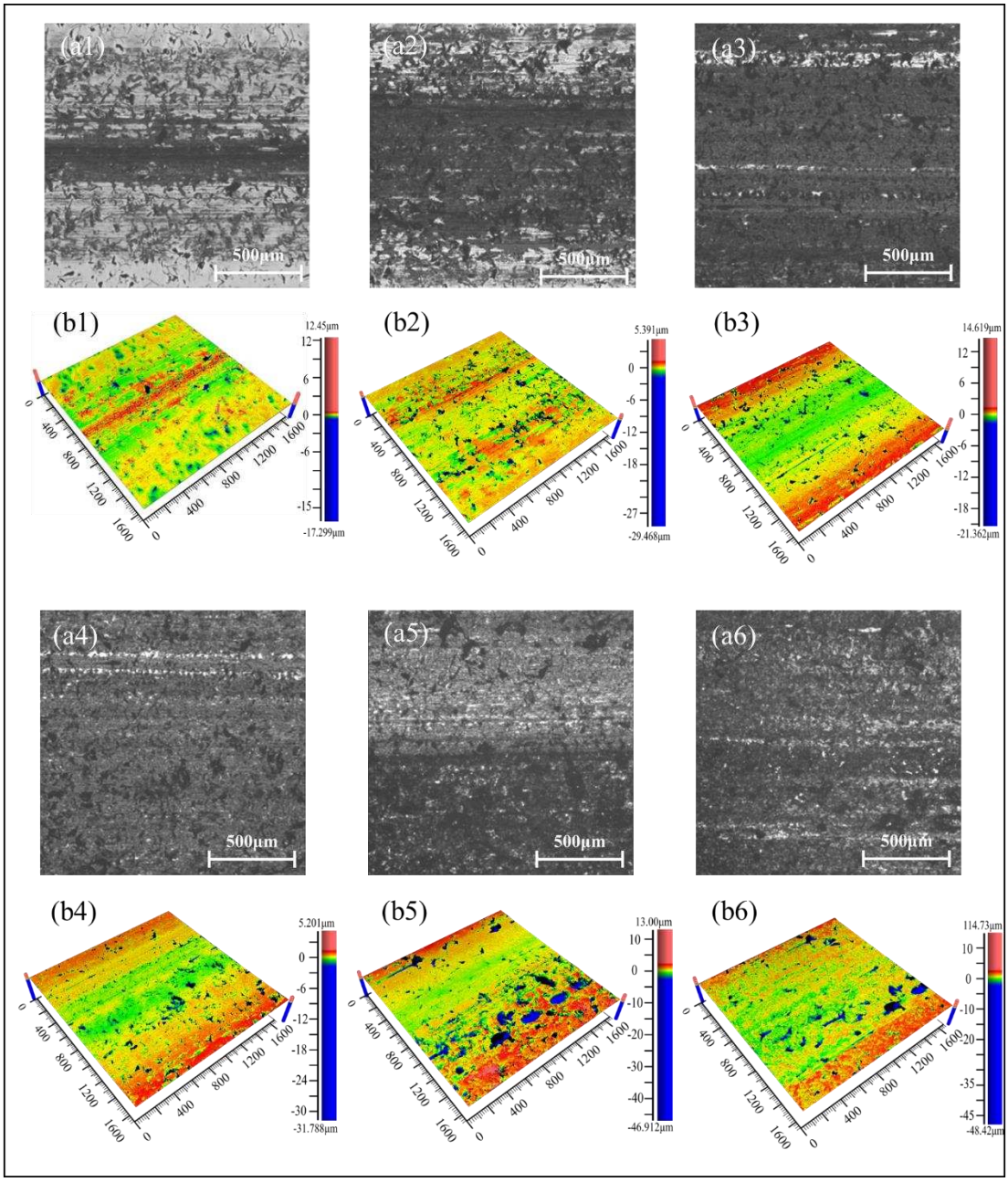

Fig. 9. Surface morphology of wear scar at different wear times: (a) two-dimensional morphology, (b) three-dimensional morphology, (1) 30 min, (2) 60 min, (3) 90 min, (4) 120 min, (5) 150 min, (6) 180 min.

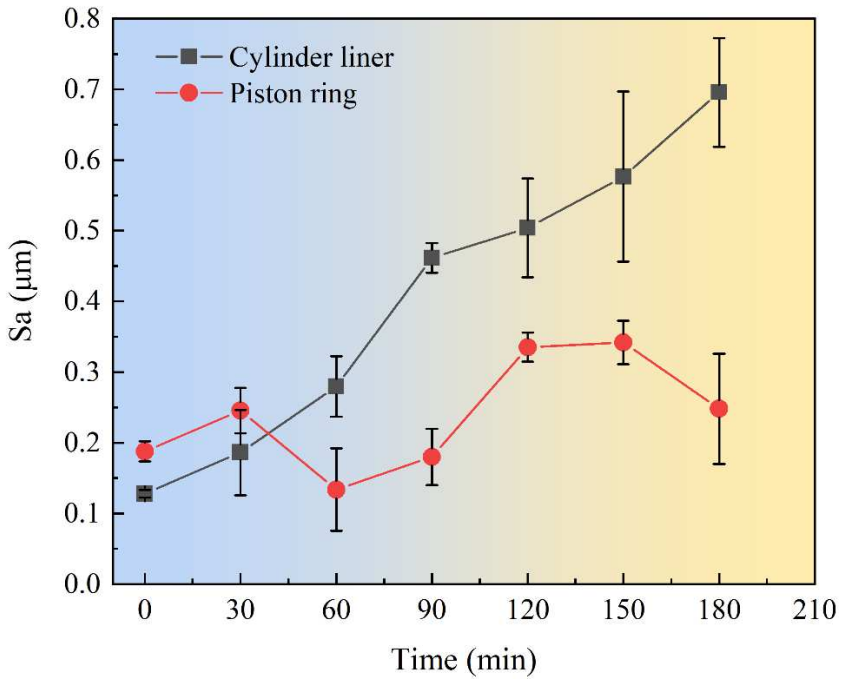

Fig. 10. Variation of surface roughness value Sa (plane arithmetic average height) of the cylinder liner and piston ring wear scars at different time.

3.4. Evolution of surface morphology

The modification in surface morphology characteristics influences the alteration in friction coefficient and wear rate. Fig. 11 depicts the wear scar morphology of the cylinder liner following a wear duration of 15 min. Evidently, the wear scar surface appears fairly sleek, with minimal signs of wear. The defects are mainly concentrated in the graphite position. Graphite has low strength, making it susceptible to detachment and the formation of defects during the wear process. The shedding of graphite also leads to the wear of the surrounding matrix structure due to the stress concentration effect (Fig. 11 (a)). This result was also confirmed in previous studies [23, 42]. In addition, a small amount of oxide layer (Fig. 11 (b)), or 'glazed layer', can be observed on the wear scar surface. The oxide layer is mainly formed by the reaction of wear debris with oxygen in the air and repeated rolling with graphite in the friction pair [14]. The oxide layer adheres to the surface of the wear scars, hindering direct contact between the piston ring and the cylinder liner and providing protection to the cylinder liner surface. Furthermore, the element distribution analysis unearths a noticeable carbon enrichment existing on the outermost layer of the oxide. It also indicates that

the exfoliated graphite entered the wear scar and mixed with the wear debris to form the glazed layer. The presence of graphite contributes to a decrease in the friction coefficient due to its lubricating properties. As the graphite overflow increases, the lubrication effect is enhanced, resulting in a decrease in the friction coefficient observed during the stage of low wear (Fig. 5 (b)). The low friction coefficient signifies a reduced friction force, consequently leading to a low wear rate.

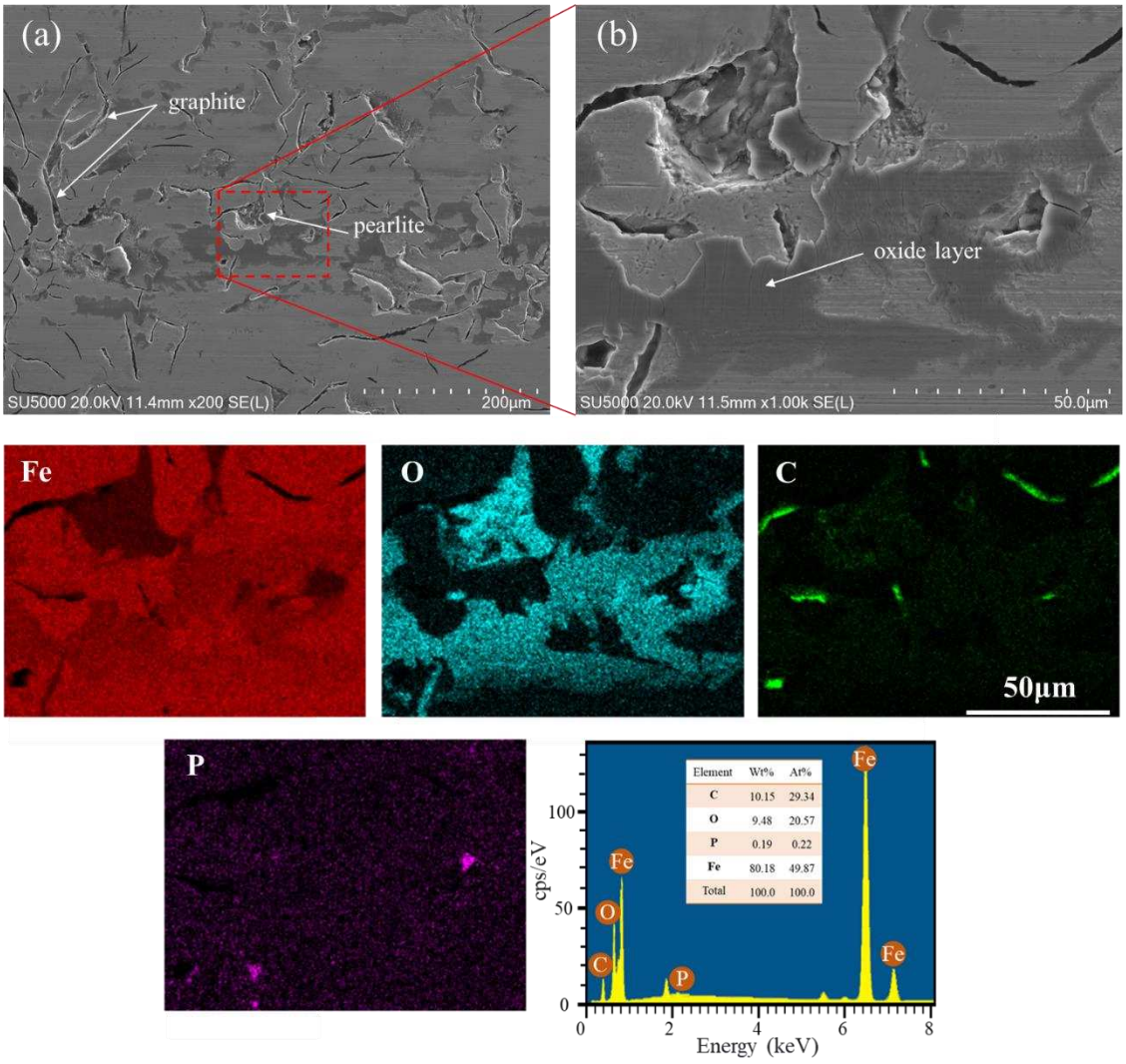

Fig. 11. Surface morphology and element distribution of wear scar after 15 min of wear: (a) surface morphology of wear scar, (b) local enlarged image and element distribution.

Fig. 12 shows the wear scar morphology at a wear time of 60 min. It can be seen that there is obvious spalling on the surface, which is the fatigue wear phenomenon of the matrix structure under repeated frictional forces. At the same time, an obvious

furrow can also be observed on the surface of the wear scar, indicating that there is abrasive wear. In addition, noticeable adhesive wear occurred at the local position of the wear scar (Fig. 12 b). The observation demonstrates that the dominant mechanism of wear during the period of stable wear is abrasive and adhesive wear. Additionally, Fig. 12 (a) illustrates that the wear debris conceals the flaws generated by graphite shedding, leading to a self-repairing phenomenon. The results of EDS analysis shows that the graphite content decreases, and the position where the graphite produces defects is rich in oxygen, indicating that the defects are covered by wear debris. It differs from the graphite closure mentioned in the previous literature [23, 37]. Due to the coverage of the graphite position, the surface self-lubricating effect decreases, resulting in a larger friction coefficient and an increase in wear rate. The location of phosphorus eutectic can be determined based on the distribution of phosphorus elements, as shown in Fig. 12 (c). The phosphorus eutectic is not covered by the oxide layer, and there is no noticeable wear. The findings of this study align with what has been reported in previous literature [5]. The phosphorus eutectic has high hardness and is difficult to remove during wear. Therefore, it can play a supporting role in the friction system, thereby improving the wear resistance of cast iron.

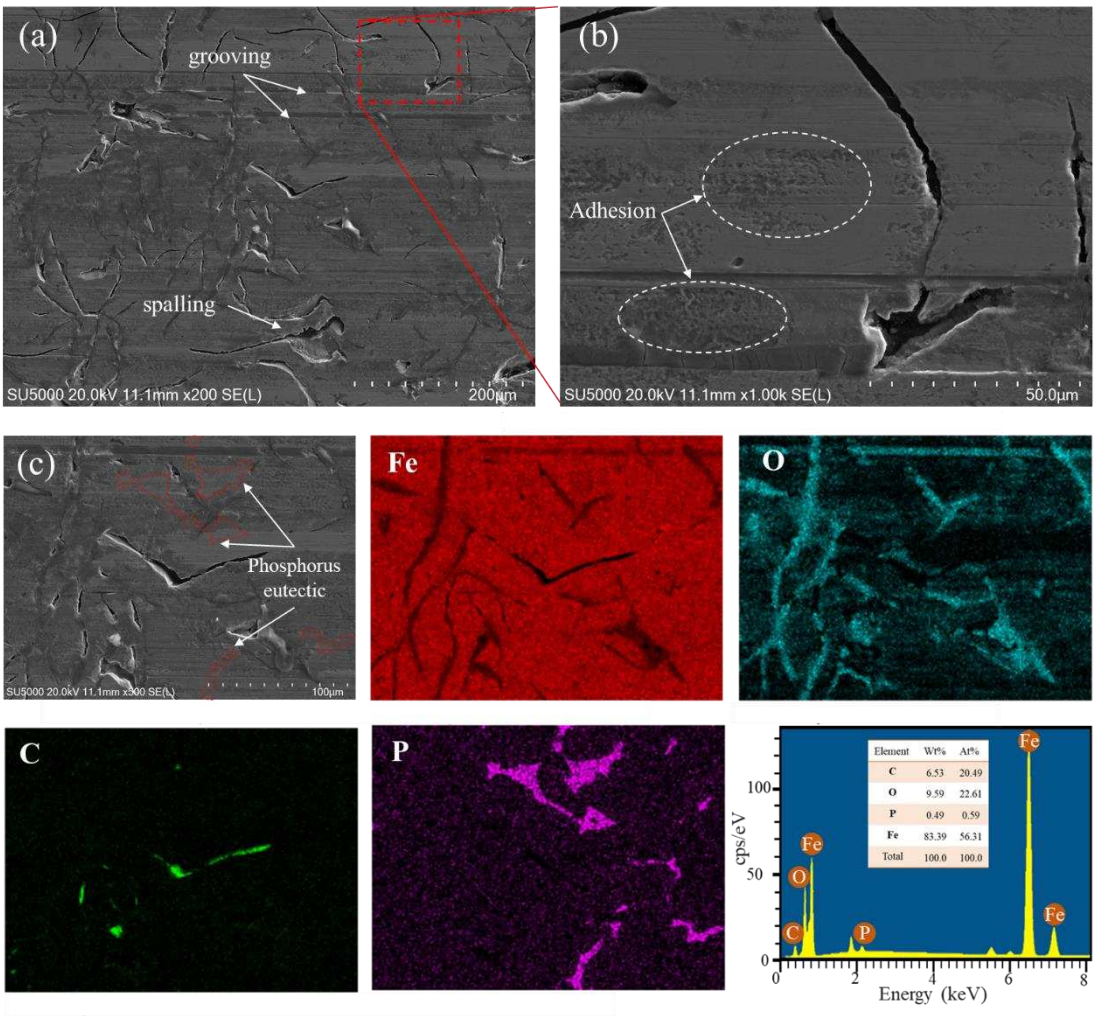

Fig. 12. Surface morphology and element distribution of wear scar when worn for 60 min: (a) surface morphology of wear scar, (b) local enlarged image, (c) local element distribution of the wear scar.

Fig. 13 shows the wear scar morphology after 180 min of wear, indicating severe wear on the surface of the wear scars. The middle position of the wear scar is smooth, but there are many cracks. There is an obvious oxide layer shedding at the periphery of the wear scar. Based on the morphology of the resulting imperfections, it can be inferred that delamination wear primarily constitutes the wear mechanism at this stage. Furthermore, from Fig. 13 (b), it is evident that multiple cracks surround the delamination wear region. These cracks propagate and intersect with one another, ultimately causing the flaking of the layered structure. The element distribution characteristics show that, after 180 min of wear, it is difficult to observe the presence of graphite on the surface (Fig. 13 (c)), indicating that the oxide layer has entirely

covered the wear scar surface and the self-lubricating effect of graphite is further weakened. The increase in oxygen content also proves that the area of the oxide layer increases. The oxygen content in the middle of the wear scar is low, possibly due to the severe wear in the middle position, and the oxide layer falls off, while the smooth surface indicates a new oxide layer is forming. In addition, it can be seen that the oxygen content at the phosphorus eutectic position is low; that is, no oxide layer is attached to the surface. Fig. 13 (c) shows that the wear degree of the phosphorus eutectic is small. The phosphorus eutectic can support the friction pair even if the surrounding matrix structure has fallen off. It also indicates that the phosphorus eutectic finally falls off during wear.

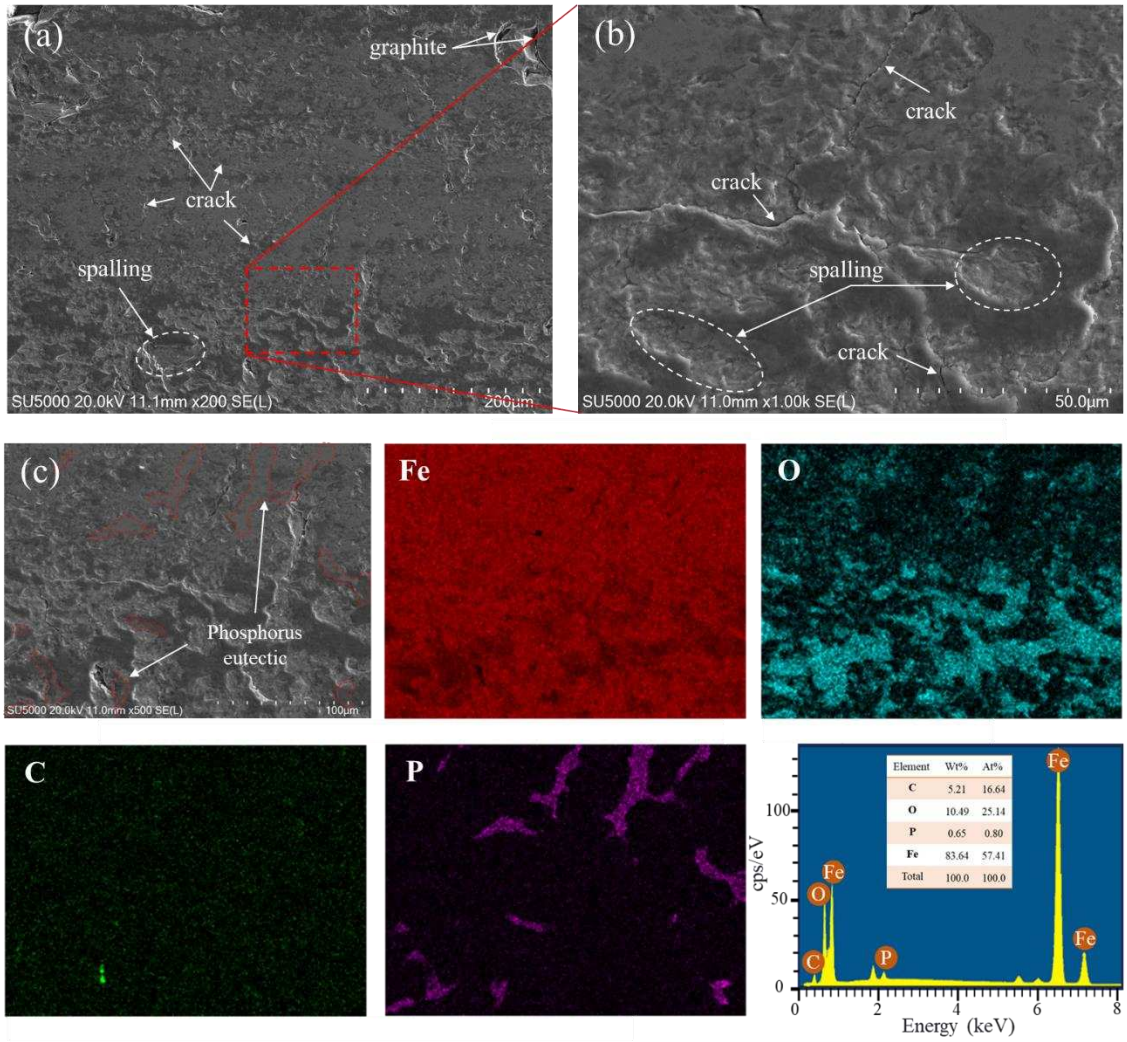

Fig. 13. Surface morphology and element distribution of wear scar when worn for 180 min: (a) surface morphology of wear scar, (b) local enlarged image, (c) local element

distribution of the wear scar.

Fig. 14 exhibits the morphological features of debris during varying wear durations. In the low-wear stage, the presence of graphite facilitates a self-lubricating phenomenon, thereby minimizing surface wear. However, due to the localized stress concentration adjacent to the graphite, slight wear is observed within the matrix structure. Consequently, the wear debris primarily comprises granular particles (Fig. 14 (a)). In the stable wear stage, adhesion wear occurs at the local position, so the wear debris mainly appears as fine granular or flocculent (Fig. 14 (b)). It also contains some sizeable granular debris, and it can be seen from the figure that there are noticeable cracks on the surface of this debris (at the red arrow position). Moreover, according to the elemental analysis of the wear debris (Fig. 14 (c)), it can be seen that there is oxygen enrichment on the surface, indicating that the larger debris mainly comes from the shedding of the oxide layer. In the severe wear stage, due to the delamination wear being the primary wear mechanism at this time, the shape of the debris presents as thin flakes (Fig. 14 (d)). Obvious cracks can also be observed at the edge of the wear debris.

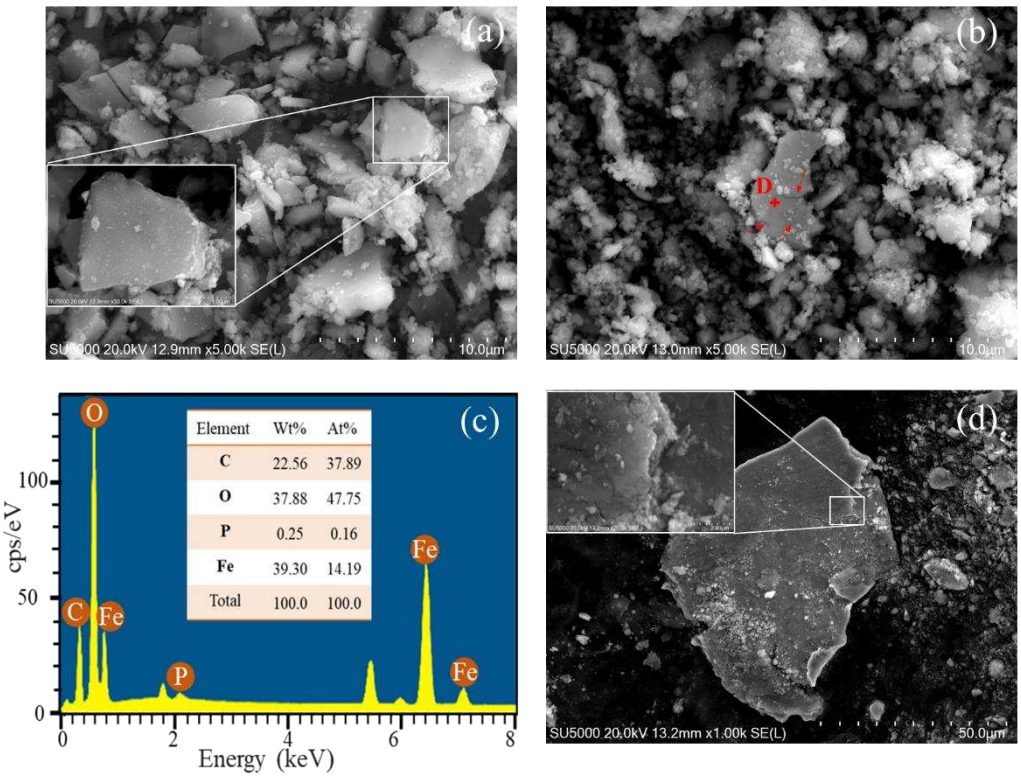

Fig. 14. Wear debris morphology and element content at different wear time: (a) 15

min, (b) 60 min, (c) the energy spectrum of point D in (b), (d) 180 min.

The surface morphology of the wear scar on the piston ring is presented in Fig. 15. The figure indicates the presence of pitting pits on the surface after a wear time of 15 min. These pits are not caused by wear but are left over during the machining process, which can also be proved in Fig. 1 (d). The compacting and accumulation of debris at the scratch demonstrate that the wear debris will likewise exert a specific restorative influence on the surface imperfection of the piston ring. When the wear time is 60 min (Fig. 15 (b)), obvious adhesive debris appears on the wear scar. That is, the cylinder liner material transfers to the surface of the piston ring, indicating that adhesive wear takes place at this time. This finding aligns with the graphical results in Fig.12 (b). When the wear time is 120 min (Fig. 15 (c)), the wear scar's surface appears fairly even, with the disappearance of the machining morphology, signifying notable wear on the piston ring. A small amount of adhesive debris can still be observed on the wear scar, indicating that the adhesion still exists. However, according to the surface morphology, the piston ring's wear mechanism has not undergone significant changes during the wear process. This result is consistent with the change in wear rate (Fig. 8).

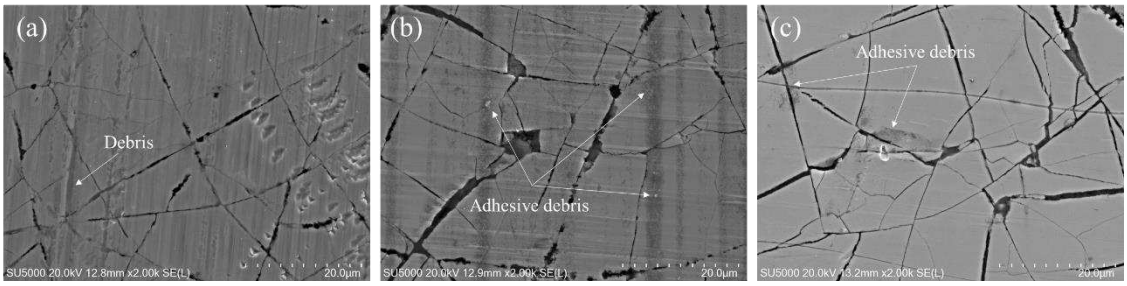

Fig. 15. The surface morphology of piston ring wear scar at different wear times: (a) 15 min, (b) 60 min, (c) 120 min.

3.5. Evolution of subsurface morphology

Fig. 16 shows the wear scar's cross-section morphology at different wear times. When the wear time is 15 min (Fig. 16 (a)), the wear scar surface is relatively flat, and only slight wear occurs at the graphite position. The microstructure around the graphite also has a slight peeling, and it is mainly pearlite. This result is consistent with the analysis of the worn surface in the previous section. It also indicates that the spalling

of graphite and a small amount of pearlite mainly occurs in the initial wear. When the wear time is 90 min (Fig. 16 (b)), it is in a stable wear state according to the friction coefficient change. Due to the increased friction force, the matrix structure began to wear seriously, and obvious spalling defects appeared. Although there is also the matrix structure spalling off at the beginning of wear (Fig. 16 (a)), it is mainly caused by the influence of graphite spalling. At this time, the matrix structure around the phosphorus eutectic is also worn. At the same time, this phenomenon also proves that phosphorus eutectic is more difficult to wear than matrix structure. In addition, it can be seen that the cracks appear at the position of the phosphorus eutectic, indicating that the phosphorus eutectic may also fall off at this time. When the wear time is 150 min (Fig. 16 (c)), significant layered defects can be observed on the surface, consistent with the morphology of the wear debris in the previous section. According to the findings, delamination is identified as the dominant wear mechanism in severe wear cases. Furthermore, significant plastic deformation is evident in the cross-section analysis (Fig. 16 c (e)), with noticeable cracks appearing where plastic deformation occurs. The expansion of the cracks will lead to the shedding of the layer. A subsurface deformation layer with approximately 2 μm thickness is formed when the wear time reaches 180 min (Fig. 16 (d)). The deformation layer may be the glazed layer formed during the friction process or a deformation layer formed by surface plastic deformation. Usually, the glazed layer only refers to the oxide layer composed of debris formed on the surface, and the plastic deformation layer on the subsurface also plays a role in the friction process, collectively referred to as the friction layer. For convenience, the following are all expressed using friction layers. The locally enlarged image (Fig. 16 d (f)) indicates that the friction layer is attached above the graphite and prevents the overflow. In addition, it can be seen from Fig. 16 d (g) that the phosphorus eutectic is at a higher position on the surface; that is, due to the wear of the matrix structure around the phosphorus eutectic, it is prominent on the surface of the wear scar, thereby supporting the friction pair.

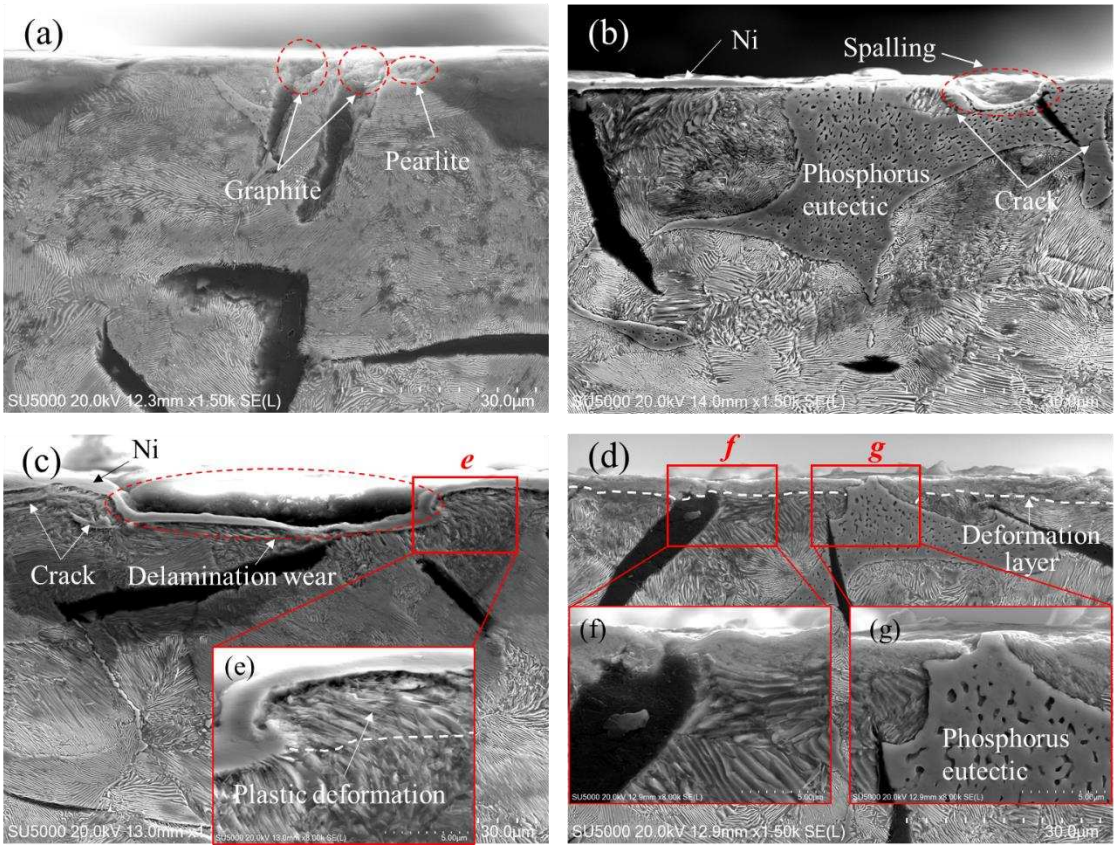

Fig. 16. The cross-section morphology of the wear scar at different wear times: (a) 15Min (b) 90 min (c) 150 min (d) 180 min (e), (f), (g) are the corresponding local enlarged graphs.

In order to further analyze the structure of the friction layer, the TEM samples were prepared by cutting the thin slices at the position of the oxide layer by focused ion beam technology (FIB), and the structural characteristics of the samples were observed by transmission electron microscopy (TEM). Fig. 17 shows the TEM image of the wear scar cross-section at a wear time of 30 min. It can be seen from the figure that there is an oxide layer with approximately 200 nm thickness attached to the surface of the wear scar, and below the oxide layer is the matrix structure of pearlite. The oxide layer is closely combined with the matrix structure, and no apparent cracks are found (Fig. 17 (b)). Further amplification of the oxide layer reveals that it mainly comprises refined grains with a 5-20 nm diameter. The analysis of the selected area electron diffraction pattern shows that the nanograins are mainly composed of Fe_2O_3 (Fig. 17 (c)). Fe_2O_3 is a highly stable iron oxide easily generated on the dry friction surface of cast iron or cast steel [53]. According to the relevant literature, the oxide layer is mainly formed by the

continuous grain refinement and reaction with oxygen under the repeated rolling action of the wear debris [47, 48]. The element distribution shows that the nanocrystalline layer is rich in C and O, which is consistent with the results in the previous section. In the initial wear stage, it is mainly the spalling of graphite and a small amount of matrix structure around it, so the generated wear debris contains a large amount of C. In addition, it can be seen that there is Cr element in the oxide layer, which may come from the coating of the piston ring, which also proves the existence of adhesive wear during the friction process.

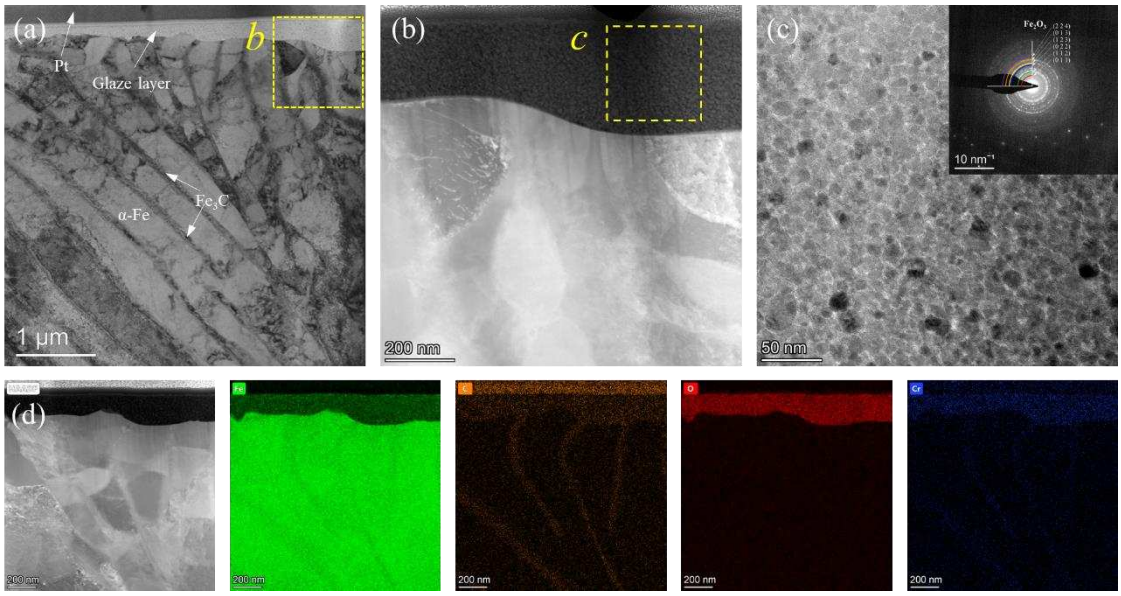

Fig. 17. Bright field scanning transmission electron microscopy (BF-STEM) image of the wear scar cross-section at a wear time of 30 min: (a) cross-section characteristics of wear scars, (b) TEM of the zone (b) defined in (a), (c) High-resolution transmission electron microscopy (HRTEM) images of the zone (c) defined in (b) and the selected area electron diffraction (SAED) pattern, (d) BF-STEM image of the wear scar cross-section and the element distribution.

Fig. 18 shows the cross-section morphology of the friction layer at 120 min. It can be seen from the figure that the subsurface structure of the wear scar is mainly divided into three layers (Fig. 18 (a)): the top nanocrystalline layer, the middle severe plastic deformation layer, and the bottom plastic deformation layer. It indicates that during the severe wear stage, the matrix structure undergoes severe plastic deformation due to the

effect of high frictional force. In addition, the thickness of the nanocrystalline layer is about 800 nm, and the grain size is within the range of 2-15 nm (Fig. 18 (b)), indicating that the nanocrystalline layer undergoes grain refinement during wear, and the thickness increases with the wear time. It also indicates that the oxide layer formed at 30 min has not yet reached the critical wear thickness [54]. According to the analysis of the selected area electron diffraction patterns of the nanocrystalline layer, it can be concluded that the nanocrystalline layer is a mixture of Fe_2O_3 and Fe_3O_4. This result is consistent with the results reported in the literature [48, 55]. However, there may be two reasons why Fe_3O_4 was not detected in the nanocrystalline layer during wear for 30 min: Firstly, there is no Fe_3O_4 in the selected limited area. Secondly, the formation conditions of Fe_2O_3 and Fe_3O_4 are different. Fe_2O_3 can be formed at sufficient oxygen concentration (atmospheric pressure) and a maximum temperature of 200 ℃ [53, 54]. The minimum friction temperature for forming Fe_3O_4 is approximately 673 K [56]. The friction coefficient at 120 min is much higher than that at 30 min, so the friction force increases under severe wear conditions, and the friction flash temperature is also higher, which reaches the formation condition of Fe_3O_4.

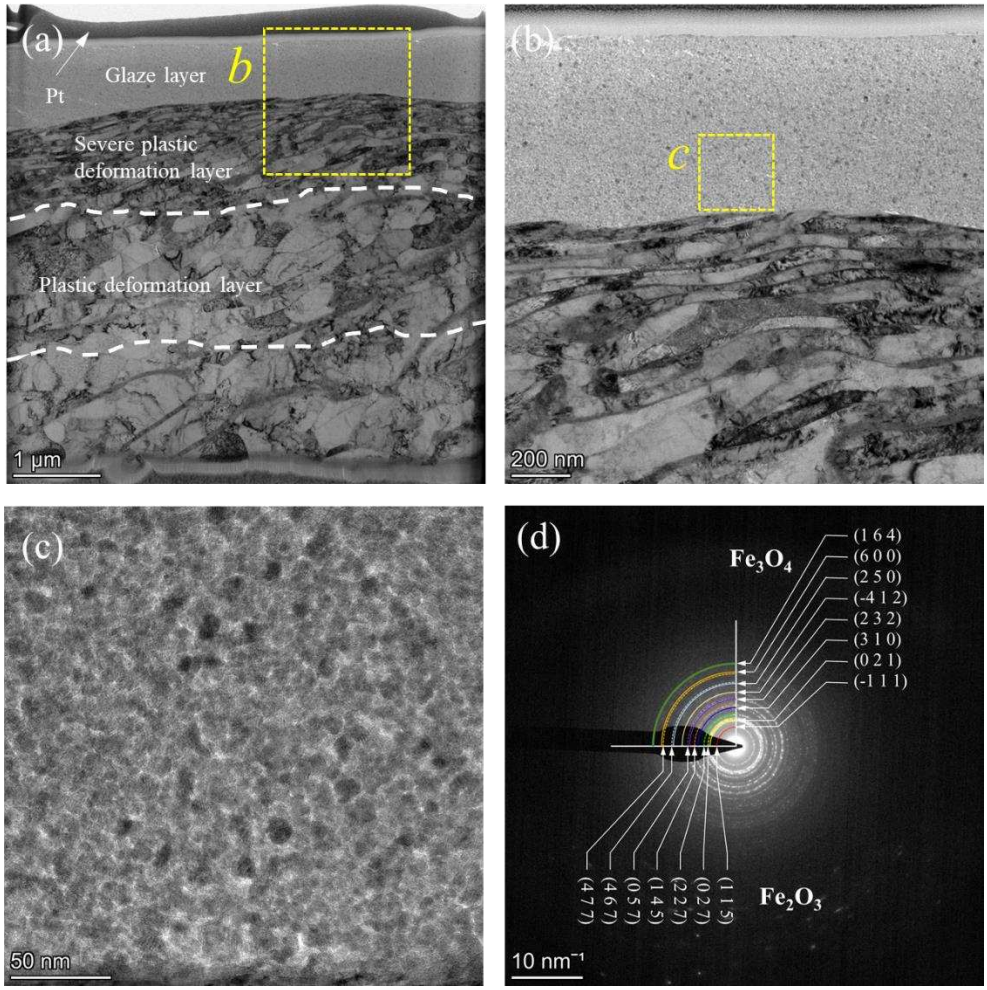

Fig. 18. (a) Bright field scanning transmission electron microscopy (BF-STEM) image of the wear scar cross-section at a wear time of 120 min: (a) cross-section characteristics of wear scars, (b) TEM of the zone (b) defined in (a), (c) HRTEM images of the zone (c) defined in (b), (d) Selected area electron diffraction (SAED) pattern of (c).

4. Discussion

According to the above analysis, it can be seen that even under the same operating parameters, the wear status of the cylinder liner and piston ring will continuously change with the wear process; that is, the cylinder liner wear process has time-varying characteristics. Based on the variation characteristics of the friction coefficient, the whole process can be divided into three wear states. The friction coefficient mainly depends on the contact characteristics between the surface asperities. In the low wear stage, due to the polishing treatment of the cylinder liner sample in this study, the

surface is smoother, and the friction coefficient is lower at the beginning of the experiment. In addition, the presence of graphite, whether embedded in the matrix or falls off into the wear scar, can reduce the friction coefficient. It is also one of the reasons why cast iron has excellent friction properties [30]. Due to the wear process, the wear debris will preferentially enter the defect position after the graphite falls off, resulting in a self-healing effect and preventing further overflow of graphite. The self-lubricating effect of graphite is weakened, and the roughness of the wear scar is also increased, which gradually increases the friction coefficient (Fig. 5 (d)). The reason for the friction coefficient reaching a stable stage again is the formation of a friction layer on the surface. This friction layer comprises nanocrystalline grains generated through the repeated rolling of wear debris. Studies have shown that nanocrystalline particles produced by steel materials during dry friction adhere to the surface, reducing the friction coefficient and causing a self-lubricating effect [47, 48]. This is also why the friction coefficient decreases in the second stable stage (Fig. 5 (c)). However, the self-lubricating effect at this time is different from the low wear stage, which mainly relies on the lubrication effect of graphite, while the former is mainly due to generating a friction layer. The area of the friction layer gradually increases with the wear process, and the self-lubricating effect of the surface is better. However, the formation and wear of the friction layer is dynamic. When the wear rate exceeds the formation rate, the friction coefficient increases obviously and enters the third stable stage. In this stage, the surface roughness increases due to the continuous shedding of the friction layer, so the friction coefficient remains at a high level. The change in friction coefficient often affects the friction flash temperature. The increase in contact temperature of the asperity during the friction process is shown in equation 14. The friction flash temperature is proportional to the friction coefficient [44]. Therefore, the flash temperature increases gradually with the friction coefficient during the wear process. The increase in temperature promotes the oxidation process, which may be one of the reasons for the increase in friction layer thickness and the formation of Fe_3O_4 (Fig. 18). The increase in friction layer thickness leads to an increase in the volume of delamination wear debris, resulting in a higher wear rate under severe wear stage.

$$\Delta T = \frac{2}{3}\frac{\mu E^* dv}{\lambda} \tag{14}$$

Where, ΔT is the temperature increase value, μ is the friction coefficient, E^* is the elastic modulus, d is the indentation depth of the asperity, v is the sliding speed, and λ is the thermal conductivity.

The wear process of cylinder liner cast iron is the shedding of the microstructures from the microscopic level. Therefore, the analysis of the wear process of the microstructures is helpful to understand better the wear state transition mechanism of the cylinder liner. In this study, the cylinder liner cast iron microstructure mainly includes graphite, pearlite, and binary phosphorus eutectic (Fig. 1 (b)). Due to the different content and mechanical properties of different microstructures, the roles in the wear process and the shedding sequence are also different [23]. According to previous research results, graphite is the first microstructure to wear off during the friction process of cast iron materials. Due to the overflow of graphite, defects are generated on the surface of the wear scar, resulting in stress concentration so that the matrix structure around the graphite is slightly spalling off (Fig. 16 (a)). As the wear process progresses, the wear debris generated by the matrix structure gradually increases. It is repeatedly rolled and adhered to the wear scar surface by the cylinder liner and piston ring, especially the defects caused by graphite overflow (Fig. 12 (a)). It is difficult for the graphite to continue to overflow. At the same time, it also makes the piston ring in direct contact with the cylinder liner matrix structure, resulting in more severe abrasive and adhesive wear. The wear of the matrix structure also leads to more wear debris entering the wear scar. According to Fig. 16 (b), the wear of the matrix structure mainly refers to the spalling of pearlite. The phosphorus eutectic is difficult to wear due to its high hardness, which makes it protrude from the wear scar surface and play a significant role in supporting the friction pair during the wear process [57]. Fig. 13 (c) shows that no oxide layer is attached to the surface of the phosphorus eutectic, which can also indicate that the phosphorus eutectic is prominent on the surface of the wear scar. Usually, the wear debris preferentially accumulates at the defect position and then reacts with oxygen to form an oxide film. The phosphorus eutectic is directly in contact with the

piston ring, so, forming a complete oxide film is difficult. With further wear, the phosphorus eutectic cracks and falls off under friction force (Fig. 16 (b)). Currently, the piston ring is in contact with the friction layer. Due to the dense nanocrystalline particles above the friction layer and their excellent mechanical properties, the crack source is mainly generated in the excessive position of the friction layer and the matrix material or in the matrix material. It expands along the friction direction, resulting in delamination wear [51, 58]. When the friction layer is worn to a certain extent, the phosphorus eutectic will be prominent on the surface again, supporting the friction pair. The debris generated during this process will also reattach to the surface of the wear scars. Repeat this process repeatedly. Due to the high surface roughness, there will be no low friction phenomenon, and the friction coefficient and wear rate remain stable. According to the above analysis of the microstructure wear process, the wear degradation process of the cylinder liner can be obtained, as shown in Fig. 19.

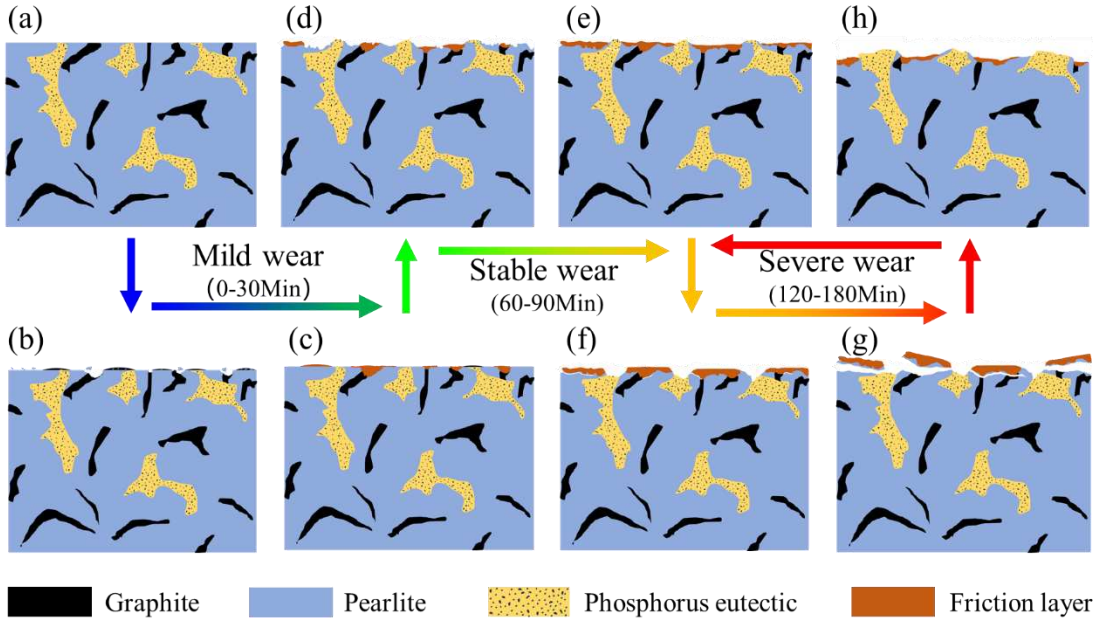

Fig. 19. Schematic diagram of the wear process of cylinder liner cast iron.

5. Conclusion

In order to analyze the time-varying wear performance and microstructure wear mechanism of cylinder liner cast iron, the dry sliding friction experiments of the cylinder liner and piston ring were carried out at room temperature. By analyzing the

friction coefficient, wear rate, and wear scar surface and interface morphology of different wear times, the conclusions are as follows:

(1) The friction coefficient increases stepwise over time during wear. It is mainly divided into the upward stage and the stable stage. The three stable stages are the low wear stage ($\mu \leq 0.3$), stable wear stage ($0.35 \leq \mu \leq 0.45$), and severe wear stage ($0.5 \leq \mu$) (μ is friction coefficient).

(2) The wear rate of the cylinder liner increases first and then stabilizes with time, and the stable value in severe wear state is about 6.5E-8. The wear rate of the piston ring gradually increases with time, but the change amplitude is small, and the average wear rate of the piston ring is about 1.4E-8, approximately 0.25 times the wear rate of the cylinder liner.

(3) In the low wear stage, the wear mechanism of the cylinder liner is the shedding of graphite and the surrounding matrix structure; the wear mechanism in the stable wear stage is mainly abrasive and adhesive wear. In the severe wear stage, the wear mechanism is mainly delamination wear.

(4) During the wear process, graphite first falls off and produces a self-lubricating effect. Then, the pearlite undergoes wear, and the generated debris reacts with oxygen to form a dense glazed layer that adheres to the surface of the wear scar, producing self-lubricating and self-healing effects. Phosphorus eutectic eventually undergoes wear, playing a supporting role in the friction process against the piston ring.

Author Statement

Baofeng Zhang: conceived and designed the experiments, performed the sample preparation, carried out the experiments and materials characterization, and prepared the manuscript. **Xuan Ma**: conceived and designed the experiments, analyzed the results, and prepared the manuscript. **Lining Liu**: conceived and designed the experiments, analyzed the results, and prepared the manuscript. **Yongqiang Wang**: analyzed the results. **Hanzhengnan Yu:** analyzed the results. **Ardian Morina:** review and edit the article. **Xiqun Lu**: acquisition of the financial support for the project leading to this study.

Declaration of competing interest

The authors declare that they have no known competing financial interests or personal relationships that could have appeared to influence the work reported in this paper.

Acknowledgments

This work was supported by the Study on Tribology and Lubrication Technology of the Marine Low-Speed Engine, the Lubrication Property Analysis and Experiment Verification of Highly-intensified Piston Assembly (No.DE0305).

Data availability

Data will be made available on request.

Reference

[1] S.C. Tung, M.L. Mcmillan, Automotive tribology overview of current advances and challenges for the future, Tribology International, 37 (2004) 517-536. https://doi.org/10.1016/j.triboint.2004.01.013

[2] K. Holmberg, P. Andersson, A. Erdemir, Global energy consumption due to friction in passenger cars, Tribology International, 47 (2012) 221-234. https://doi.org/10.1016/j.triboint.2011.11.022

[3] S. Dahdah, N. Biboulet, A. Lubrecht, P. Charles, Scuffing initiation caused by local starvation in a piston ring cylinder liner contact, Tribology International, 172 (2022) 107616. https://doi.org/10.1016/j.triboint.2022.107616

[4] P. Olander, P. Hollman, S. Jacobson, Piston ring and cylinder liner wear aggravation caused by transition to greener ship transports–Comparison of samples from test rig and field, Wear 302 (2013) 1345-1350. https://doi.org/10.1016/j.wear.2012.12.028

[5] J. Nadel, T.S. Eyre, Cylinder liner wear in low speed diesel engines, Tribology International, 11 (1978) 267-271. https://doi.org/10.1016/0301-679X(78)90056-7

[6] P. Papadopoulos, M. Priest, W. Rainforth, Investigation of fundamental wear mechanisms at the piston ring and cylinder wall interface in internal combustion engine, Proceedings of the Institution of Mechanical Engineers, Part J: Journal of Engineering Tribology, 221 (2007) 333-343. https://doi.org/10.1243/13506501JET254

[7] K. Kusumoto, K. Shimizu, V.G. Efremenko, H. Hara, M. Shirai, J. ito, M. Hatate, Y. gaqi, R.H. Purba, Three body type abrasive wear characteristics of multi-component white cast irons, Wear 426-427 (2019) 122-127. https://doi.org/10.1016/j.wear.2019.01.108

[8] E. Hu, X. Hu, T. Liu, L. Fang, K.D. Dearn, H. Xu, The role of soot particles in the tribological behavior of engine lubricating oils, Wear, 304 (2013) 152-161. https://doi.org/10.1016/j.wear.2013.05.002

[9] P. Oungpakornkaew, P. Karin, R. Tongsri, K. Hanamura, Characterization of biodiesel and soot contamination on four-ball wear mechanisms using electron

microscopy and confocal laser scanning microscopy, Wear, 458-459 (2020) 203407. https://doi.org/10.1016/j.wear.2020.203407

[10] B. Fan, B. Lia, S. Feng, J. Mao, Y.B. Xie, Modeling and experimental investigations on the relationship between wear debris concentration and wear rate in lubrication systems, Tribology International, 109 (2017) 114-123. https://doi.org/10.1016/j.triboint.2016.12.015

[11] X. Hou, Y. Wang, L. Dai, Y. Yang, J. Du, Y. Wang, H. Wan, Study on the corrosion and wear behaviors of cylinder liner in marine diesel engine burning low sulfur fuel oil, Engineering Failure Analysis, 147 (2023) 107151. https://doi.org/10.1016/j.engfailanal.2023.107151

[12] R. Cordtz, S. Mayer, S.S. Eskildsen, J. Schramm, Modeling the condensation of sulfuric acid and water on the cylinder liner of a large two-stroke marine diesel engine, Journal of Marine Science and Technology, 23 (2018) 178-187. https://doi.org/10.1007/s00773-017-0455-9

[13] J.C. Walker, Z. Barnes, A. Shehata, P. Jiang, T.J. Kamps, Variable pressure scuffing of a flake graphite cast iron diesel cylinder liner, Tribology International, 179 (2023) 108155. https://doi.org/10.1016/j.triboint.2022.108155

[14] R.S. Montgomery, Run-in and glaze formation on gray cast iron surfaces, Wear, 14 (1969) 99-105. https://doi.org/10.1016/0043-1648(69)90340-8

[15] T.F.J. Quinn, Review of oxidational wear: Part I: The origins of oxidational wear, Tribology International, 16 (1983) 257-271. https://doi.org/10.1016/0301-679X(83)90086-5

[16] B. Podgornik, Adhesive Wear Failures, Journal of failure analysis and prevention 22 (2022) 113-138. https://doi.org/10.1007/s11668-021-01322-4

[17] J. Burwell, C. Strang, On the Empirical Law of Adhesive Wear, Journal of Applied Physics, 23 (1952) 18-28. https://doi.org/10.1063/1.1701970

[18] R. Barunovic, V. Haas, C. Langlade, C.E. Krill Iii, Sliding wear of 100Cr6 in a diesel-lubricated flat–flat contact under realistic loads, Tribology International, 53 (2012) 1-11. https://doi.org/10.1016/j.triboint.2012.03.019

[19] Z.Q. Wang, J.J. Xu, Tribology in piston ring cylinder liner system of diesel

engine, Science Press, Beijing, 2021.

[20] S. Weitao, W. Bin, L. Xiaoliang, W. Yuqian, Z. Jian, Controlling the tribology performance of gray cast iron by tailoring the microstructure, Tribology International, 167 (2022) 107343. https://doi.org/10.1016/j.triboint.2021.107343

[21] A.R. Ghaderi, M. Nili Ahmadabadi, H.M. Ghasemi, Effect of graphite morphologies on the tribological behavior of austempered cast iron, Wear, 255 (2003) 410-416. https://doi.org/10.1016/S0043-1648(03)00156-X

[22] J. Keller, V. Fridrici, P. Kapsa, S. Vidaller, J.F. Huard, Influence of chemical composition and microstructure of gray cast iron on wear of heavy duty diesel engines cylinder liners, Wear, 263 (2007) 1158-1164. https://doi.org/10.1016/j.wear.2007.01.091

[23] B.F. Zhang, X. Ma, X.Q. Lu, Y. Song, Y.F. Shi, Y.D. Fu, Effect of cylinder liner cast iron microstructure on friction and wear process, Materials Science and Technology. https://doi.org/10.1080/02670836.2022.2130519

[24] B. Narayanaswamy, P. Hodgson, H. Beladi, Comparisons of the two-body abrasive wear behaviour of four different ferrous microstructures with similar hardness levels, Wear, 350-351 (2016) 155-165. https://doi.org/10.1016/j.wear.2016.01.013

[25] K. Mishra, A. Pachauri, A. Singh, Deformation, Wear and Microstructural Evolution of Nano-structured Pearlite Under Repeated Contact Sliding, Tribology Letters, 66 (2018) 109. https://doi.org/10.1007/s11249-018-1064-4

[26] X.C. Li, H.H. Ding, W.J. Wang, J. Guo, Q.Y. Liu, Z.R. Zhou, Investigation on the relationship between microstructure and wear characteristic of rail materials, Tribology International, 163 (2021) 107152. https://doi.org/10.1016/j.triboint.2021.107152

[27] R. Pan, R. Ren, X. Zhao, C. Chen, Influence of microstructure evolution during the sliding wear of CL65 steel, Wear, 400-401 (2018) 169-176. https://doi.org/10.1016/j.wear.2018.01.005

[28] E. Chya, D. Yllbc, L. Yu, L. Wei, Y. Ming, Formation of a self-lubricating layer by oxidation and solid-state amorphization of nano-lamellar microstructures during

dry sliding wear tests, Acta Materialia, 166 (2019) 208-220. https://doi.org/10.1016/j.actamat.2018.12.049

[29] J. Sugishita, S. Fujiyoshi, The Effect of cast iron graphites on friction and wear performance I: Graphite film formation on grey cast iron surfaces, Wear, 66 (1981) 209-221. https://doi.org/10.1016/0043-1648(81)90115-0

[30] A. Hase, Visualization of the tribological behavior of graphite in cast iron by in situ observations of sliding interfaces, Tribology International, 138 (2019) 40-46. https://doi.org/10.1016/j.triboint.2019.05.031

[31] Y.B. Liu, S.C. Lim, S. Ray, P.K. Rohatgi, Friction and wear of aluminium-graphite composites: the smearing process of graphite during sliding, Wear, 159 (1992) 201-205. https://doi.org/10.1016/0043-1648(92)90303-P

[32] J. Wan, D.C. Van Aken, J. Qing, T.J. Yaniak, T.E. Clements, M. Xu, Developing a graphitic white iron for abrasive wear application: Thermal and wear properties, Wear, 436-437 (2019) 202967. https://doi.org/10.1016/j.wear.2019.202967

[33] T. Matsushita, A.G. Saro, L. Elmquist, A.E.W. Jarfors, On the thermal conductivity of CGI and SGI cast irons, International Journal of Cast Metals Research, 31 (2018) 135-143. https://doi.org/10.1080/13640461.2017.1379263

[34] D.M. Holmgren, A. Diószegi, I.L. Svensson, Effects of transition from lamellar to compacted graphite on thermal conductivity of cast iron, International Journal of Cast Metals Research, 19 (2006) 303-313. https://doi.org/10.1179/136404607X176203

[35] V. Di Cocco, F. Iacoviello, M. Cavallini, Damaging micromechanisms characterization of a ferritic ductile cast iron, Engineering Fracture Mechanics, 77 (2010) 2016-2023. https://doi.org/10.1016/j.engfracmech.2010.03.037

[36] K. Masuda, N. Oguma, M. Ishiguro, Y. Sakamoto, S. Ishihara, Sliding wear life and sliding wear mechanism of gray cast iron AISI NO.35B, Wear, 474-475 (2021) 203870. https://doi.org/10.1016/j.wear.2021.203870

[37] R. Ghasemi, L. Elmquist, The relationship between flake graphite orientation, smearing Effect, and closing tendency under abrasive wear conditions, Wear, 317 (2014) 153-162. https://doi.org/10.1016/j.wear.2014.05.015

[38] A. Bedolla-Jacuinde, F.V. Guerra, A.J. Guerrero-Pastran, M.A. Sierra-Cetina, S. Valdez-Medina, Microstructural Effect and wear performance of high chromium white cast iron modified with high boron contents, Wear, 476 (2021) 203675. https://doi.org/10.1016/j.wear.2021.203675

[39] H.R. Abbasi, M. Bazdar, A. Halvaee, Effect of phosphorus as an alloying element on microstructure and mechanical properties of pearlitic gray cast iron, Materials Science and Engineering: A, 444 (2007) 314-317. https://doi.org/10.1016/j.msea.2006.08.108

[40] R.H. Purba, K. Shimizu, K. Kusumoto, Y. Gaqi, T. Todaka, Effect of boron addition on three-body abrasive wear characteristics of high chromium based multi-component white cast iron, Materials Chemistry and Physics, 275 (2022) 125232. https://doi.org/10.1016/j.matchemphys.2021.125232

[41] N.S.M. Committee, Metallographic test for grey cast iron, National Standardization Management Committee, National Standardization Management Committee, 2023.

[42] B. Zhang, X. Ma, L. Liu, H. Yu, A. Morina, X. Lu, Study on the sliding wear map of cylinder liner − piston ring based on various operating parameters, Tribology International, 186 (2023) 108632. https://doi.org/10.1016/j.triboint.2023.108632

[43] C.D. Rakopoulos, E.G. Giakoumis, D.C. Rakopoulos, Cylinder wall temperature effects on the transient performance of a turbocharged Diesel engine, Energy Conversion and Management, 45 (2004) 2627-2638. https://doi.org/10.1016/j.enconman.2003.12.014

[44] V. Popov, Contact Mechanics and Friction: Physical Principles and Applications, 2010.

[45] S. Johansson, P.H. Nilsson, R. Ohlsson, B.-G. Rosén, Experimental friction evaluation of cylinder liner/piston ring contact, Wear, 271 (2011) 625-633. https://doi.org/10.1016/j.wear.2010.08.028

[46] J.J. Truhan, J. Qu, P.J. Blau, A rig test to measure friction and wear of heavy duty diesel engine piston rings and cylinder liners using realistic lubricants, Tribology International, 38 (2005) 211-218. https://doi.org/10.1016/j.triboint.2004.08.003

[47] C. Li, X. Deng, Z. Wang, Friction behaviour and self-lubricating mechanism of low alloy martensitic steel during reciprocating sliding, Wear, 482-483 (2021) 203972. https://doi.org/10.1016/j.wear.2021.203972

[48] C.-h. Yin, Y.-l. Liang, Y. Liang, W. Li, M. Yang, Formation of a self-lubricating layer by oxidation and solid-state amorphization of nano-lamellar microstructures during dry sliding wear tests, Acta Materialia, 166 (2019) 208-220. https://doi.org/10.1016/j.actamat.2018.12.049

[49] J.J. Truhan, J. Qu, P.J.J.T.I. Blau, A rig test to measure friction and wear of heavy duty diesel engine piston rings and cylinder liners using realistic lubricants, Tribology International, 38 (2005) 211-218. https://doi.org/10.1016/j.triboint.2004.08.003

[50] N.B. Dhokey, R.K.J.W. Paretkar, Study of wear mechanisms in copper-based SiC p (20% by volume) reinforced composite, Wear, 265 (2008) 117-133. https://doi.org/10.1016/j.wear.2007.09.001

[51] F. Zhang, G. Yu, S. Yan, J. Chen, L. Wang, F. Yin, Influence of Al content and post-annealing on synthesis and mechanical properties of plasma sprayed Cr–Al–C composite coatings, Ceramics International, 48 (2022) 17343-17351. https://doi.org/10.1016/j.ceramint.2022.02.297

[52] F. Ficici, S. Kurgun, Analysis of Weight loss in Reciprocating Wear Test of Cylinder Liner and Piston Ring Coated with Molybdenum, Arabian Journal for Science and Engineering, 46 (2021) 7801-7813. https://doi.org/10.1007/s13369-021-05566-y

[53] X.H. Cui, S.Q. Wang, F. Wang, K.M. Chen, Research on oxidation wear mechanism of the cast steels, Wear, 265 (2008) 468-476. https://doi.org/10.1016/j.wear.2007.11.015

[54] F.H. Stott, The role of oxidation in the wear of alloys, Tribology International, 31 (1998) 61-71. https://doi.org/10.1016/S0301-679X(98)00008-5

[55] F. Saeidi, A.A. Taylor, B. Meylan, P. Hoffmann, K. Wasmer, Origin of scuffing in grey cast iron-steel tribo-system, Materials & Design, 116 (2017) 622-630. https://doi.org/10.1016/j.matdes.2016.12.044

[56] T.F.J. Quinn, J.L. Sullivan, D.M. Rowson, Origins and development of

oxidational wear at low ambient temperatures, Wear, 94 (1984) 175-191. https://doi.org/10.1016/0043-1648(84)90053-X

[57] W.J. Tomlinson, G. Dennison, Effect of phosphide and matrix microstructures on the dry sliding wear of grey cast iron, Tribology International, 22 (1989) 259-264. https://doi.org/10.1016/0301-679X(89)90084-4

[58] N. P. Suh, The delamination theory of wear, Wear, 25 (1973) 111-124. https://doi.org/10.1016/0043-1648(73)90125-7